Manuscript Details

https://doi.org/10.1016/j.oregeorev.2018.02.001

Manuscript number	ORGEO_2017_664
Title	Major and trace elements geochemistry of emerald from several deposits: Implications for genetic models and classification schemes
Article type	Research paper

Abstract

In the present work, we report the chemical composition of representative emerald crystals from some of the most important worldwide deposits. Major and trace elements were investigated using Electron Microprobe Analysis (EMPA) and Secondary Ion Mass Spectrometry (SIMS) techniques. Binary and spider diagrams along with statistical analysis, i.e., Principal Component Analysis (PCA), were used to discriminate each deposit with high reliability. PCA of SiO2, Al2O3, V, Sc, B, Li content identified distinct groups. Moreover, spider and binary diagrams, involving Cs, Rb, B, Li, Cr, V, Sc data, highlighted additional peculiarities among emerald crystals not discriminated by PCA. The results of this study can contribute to identify useful geochemical markers for provenance purpose.

Keywords	Deposits, EMPA, SIMS, PCA, Provenance
Corresponding Author	Caterina De Vito
Corresponding Author's Institution	Sapienza University of Rome
Order of Authors	Carlo Aurisicchio, Aida Maria Conte, Laura Medeghini, Luisa Ottolini, Caterina De Vito
Suggested reviewers	Marc Chaussidon, Lee A. Groat, David Schwartz, Gaston Giuliani

Submission Files Included in this PDF

File Name [File Type]

Cover Letter.docx [Cover Letter]

Highlights.docx [Highlights]

Graphical Abstract.tif [Graphical Abstract]

Manuscript File.docx [Manuscript File]

Figure_1.tiff [Figure]

Figure_2.tif [Figure]

Figure_3.tif [Figure]

Figure_4.tif [Figure]

Figure_5.tif [Figure]

Figure_6a.tif [Figure]

Figure_6b.tif [Figure]

Figure_7.tif [Figure]

Figure_8.tif [Figure]

Figure_9.tif [Figure]

Figure_10.tif [Figure]

Figure_11.tif [Figure]

Figure_12.tif [Figure]

Submission Files Not Included in this PDF

File Name [File Type]

Table_1.xls [Table]

Table_S1.xlsx [Table]

To view all the submission files, including those not included in the PDF, click on the manuscript title on your EVISE Homepage, then click 'Download zip file'.

Research Data Related to this Submission

There are no linked research data sets for this submission. The following reason is given:
Data will be made available on request

Dear Editor,

Please consider the manuscript “Major and trace elements geochemistry of emerald from several deposits: Implications for genetic models and classification schemes” by *Carlo Aurisicchio, Aida Maria Conte, Laura Medeghini, Luisa Ottolini and Caterina De Vito* for the publication in Ore Geology Reviews.

The manuscript reports the results of a multi-analytical approach (i.e., Electron Microprobe Analysis (EMPA), Secondary Ion Mass Spectrometry (SIMS)and statistical treatments (PCA) used to characterize emerald crystals from different deposits.

The aim of this work is to individuate geochemical markers useful to differentiate crystals from different deposits. Moreover, a deep geochemical linvestigation of each crystal and the statistic treatment of the data were done. In addition, we discuss the chemical features of the crystals considering the environment of emerald formation.

The novelty of this manuscript lies not only in providing to the reader a complete chemical characterization of the samples but also major and trace elements statistical treatment may be useful to improve existing genetic models of emerald deposits and in turn classification schemes.

We look forward to your positive response.

Yours sincerely,

Caterina De Vito

Major and trace elements were investigated using Electron Microprobe Analysis (EMPA) and Secondary Ion Mass Spectrometry (SIMS) techniques

Binary and spider diagrams and Principal Component Analysis (PCA), were used to discriminate among crystals

The results of this study can contribute to identify useful geochemical markers

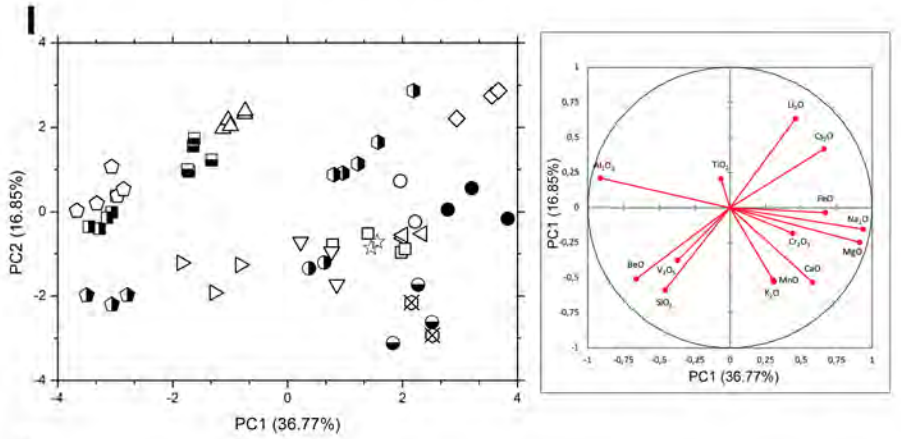

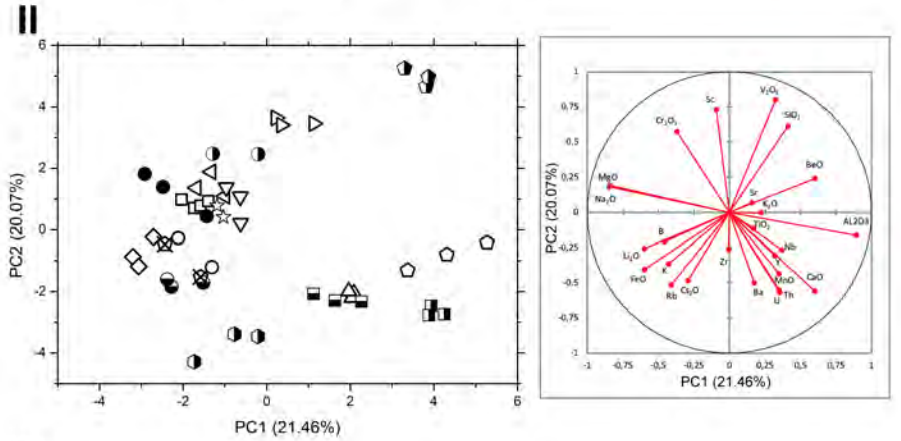

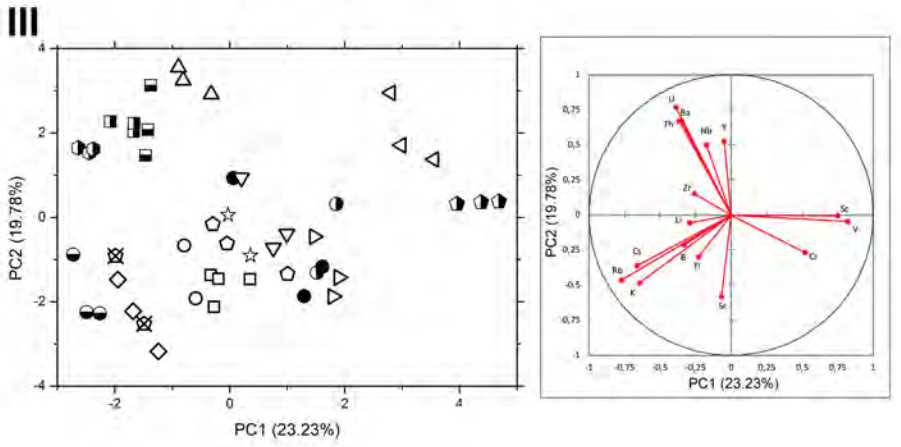

- Afghanistan (Pajshir Valley)
- Australia (Poona)
- Austria (Habachtal)
- Brazil (St. Terezinha)
- Colombia (Muzo)
- Egypt (Sikait)
- Egypt (Zabara)
- Ethiopia (Kenticha)
- India (Rajghar)
- Madagascar (Mananjary)
- Mozambique (Alto Ligonha)
- Nigeria (Jos)
- Pakistan (Swat Valley)
- Russia (Malyshevsk)
- Tanzania (Sumbawanga)
- Zambia (Kitwe)
- Zimbabwe (Sandawana)

Major and trace elements geochemistry of emerald from several deposits: Implications for genetic models and classification schemes

Carlo Aurisicchio[a], Aida M. Conte[a], Laura Medeghini[b], Luisa Ottolini[c], Caterina De Vito[b*]

[1]CNR – Istituto di Geoscienze e Georisorse, Sede Secondaria di Roma, Piazzale A. Moro 5, I–00185 Roma, Italy
[2]Dipartimento di Scienze della Terra, Sapienza Università di Roma, Piazzale A. Moro 5, I–00185 Roma, Italy
[3]CNR – Istituto di Geoscienze e Georisorse, Sede Secondaria di Pavia, Via A. Ferrata 1, I–27100 Pavia, Italy

Corresponding author: Caterina De Vito, caterina.devito@uniroma1.it, +39 06 49914893

Abstract

In the present work, we report the chemical composition of representative emerald crystals from some of the most important worldwide deposits. Major and trace elements were investigated using Electron Microprobe Analysis (EMPA) and Secondary Ion Mass Spectrometry (SIMS) techniques. Binary and spider diagrams along with statistical analysis, i.e., Principal Component Analysis (PCA), were used to discriminate each deposit with high reliability. PCA of SiO_2, Al_2O_3, V, Sc, B, Li content identified distinct groups. Moreover, spider and binary diagrams, involving Cs, Rb, B, Li, Cr, V, Sc data, highlighted additional peculiarities among emerald crystals not discriminated by PCA. The results of this study can contribute to identify useful geochemical markers for provenance purpose.

Keywords: Emerald, Deposits, EMPA, SIMS, PCA, Provenance

1 Introduction

Since ancient times, the mining and exchange of emerald have been playing a key role in the history of civilizations. The widespread diffusion of this gem very far from its deposit highlights the historical importance of emerald in the economic and religious structures of ancient cultures. Consequently, studies aimed at linking each gemstone to its source (i.e., provenance) continue to be a central topic for geologists, gemologists, archaeologists, historians, and others.

Emerald belongs to beryl-group minerals with general formula ($Be_3Al_2Si_6O_{18}$), where tetrahedra form six-member rings filled by Si (T2), whereas Al and Be ions are located at the octahedral (O) and tetrahedral (T1) sites, respectively,

which links together the columns of rings of six Si–O tetrahedra. Several distinct substitutions occur at the octahedral (O) and the tetrahedral (T1, T2) sites giving rise to different varieties. More details about beryl structure are reported in numerous studies (Artioli et al., 1993; Aurisicchio et al., 1988).

Emerald, the green variety of beryl, owes its color to the presence of Cr and/or V and/or Sc, which replace Al in the octahedral site. The concentration of these transitional chromophore elements (CTE) is typically in the range of minor or trace elements (e.g., Groat et al., 2008**).**

Nowadays, the scientific community is involved to contribute in solving the existing debate about the genetic classification schemes of emerald deposits. In his review, Groat et al. (2008) summarize the different genetic models proposed for emerald formation (Barton and Young, 2002; Dereppe et al., 2000; Gavrilenko, 2003; Gavrilenko and Dashevsky, 1998; Schwarz and Giuliani, 2001; Schwarz et al., 2001), resulting in two main types of classification schemes. The first one, based on geological-mineralogical characterization (Schwarz and Giuliani, 2001), distinguishes the emerald deposits related to granite-pegmatite intrusion from those controlled by tectonic structures. The second one, based on the major element chemistry of more than 450 emerald crystals, groups the worldwide deposits in five distinct categories using the Artificial Neural Networks (ANN) data processing (Dereppe et al., 2000).

Zwaan (2006) observed that a considerable number of emerald deposits cannot be unambiguously classified using the existing schemes, and suggested a classification based also on trace elements geochemistry. Two preliminary studies (Aurisicchio et al., 2007; McManus et al., 2004;) reported trace element compositions of emeralds from different deposits using ICP-MS/LIBS (Inductively Coupled Plasma Mass Spectrometry/Laser-Induced Breakdown Spectroscopy) and SIMS techniques, respectively.

Here we present and discuss the behaviors of major, minor and trace elements of emerald samples from the most important worldwide deposits, some of them never investigated before. The use of EMP and SIMS analysis along with statistical treatment (PCA) permits to find geochemical markers useful for discrimination. In addition, we try to link the geochemical features of each group to the geological environment and, in turn, to the genetic processes leading to emerald formation.

2 Geological backgrounds of emerald deposits

The emerald crystallization is mainly related to metasomatic processes caused by fluids originating in different geological contexts, which induce the mobilization of elements like Be, Cr, Sc and V.

Based on the classification schemes of Schwarz and Giuliani (2001) the studied emeralds belonging to Type-1 and Type-2 deposits, are listed as follows.

2.1 Type-1 deposits

The emerald district of Poona (Australia), related to felsic intrusions inside basic rocks, occurs in a phlogopite "blackwall" zone, suggesting metasomatic reactions (under low-grade metamorphic conditions) between pre-existing quartz–muscovite or quartz–topaz greisens and ultramafic bodies (Grundmann and Morteani, 1995; Kazmi and Snee, 1989; Mumme, 1982). Light, green emerald occurs with ruby, chrysoberyl ($BeAl_2O_4$), sapphire, topaz, fluorite, margarite, muscovite, phenakite (Be_2SiO_4), bromellite (BeO) and quartz within micaceous veinlets.

The genesis of Malyshevsk emerald district (in the eastern slope of the Middle Urals) (Grundmann and Giuliani, 2002; Kupriyanova, 2002) is related to magmatic-hydrothermal (granite-related) processes. Emerald crystallization occurs at the contact between granite and talc schists/talc–actinolite schists (Fersmann, 1929) into pegmatitic pockets, resulting from the interaction between felsic melt and Cr released from country rocks. Emerald occurs with chrysoberyl ($BeAl_2O_4$), phenakite (Be_2SiO_4) and bromellite (BeO) in metasomatic veins (Pekov, 1998).

In the district of Mananjary deposit (Madagascar) emerald crystals are hosted in the phlogopite-bearing contact zones, between pegmatite and surrounding Cr-bearing basic-ultrabasic rocks (Dill, 2015). The infiltration of F-rich fluids in the country rocks activates metasomatic reactions, involving the co- precipitation of F-rich phlogopite and emerald, which contains up to 2500 ppm Cr (Moine et al., 2004).

In the Alto Ligonha Province (northern Mozambique) beryl is an accessory mineral in K-enriched pegmatites (Cronwright, 2005; Dill, 2015; Schmidt, 1986; Thomas and Davidso, 2010) occurring in fine-grained gneiss, schist, granulite, migmatite and magmatic intrusion of pre-Karoo age. The genetic model for pegmatite containing emerald (Maria III and Niane) involves the intrusion of granitic pegmatites within Cr-V-bearing basic-ultrabasic rocks (Dias and Wilson, 2000). The emerald from Nigeria is the result of early metasomatic albitization of alkaline granite of the Mesozoic Jos ring complex (Vapnik and Moroz, 2000). Emerald along with quartz, feldspar, and topaz occur in small pegmatite pockets (up to 8 cm in size) at the contact granite-country rock, near the Nigerian Basement Complex; Cr was likely incorporated from the basement or younger volcanic rocks (Schwarz et al., 1996).

The Sumbawanga deposit is in western Tanzania (near the Lake Rukwa). The emerald is hosted within a weathered basic host rocks penetrated by granitic intrusions (Moroz et al., 2001; Themelis, 1989;). However, its genetic model is still under debate (Moroz et al., 2001).

The emerald mines from Zambia are in the Kafubu area (Kitwe). The deposits are hosted by Cr-rich (3000 to 4000 ppm) talc-chlorite±actinolite±magnetite metabasites of the metamorphosed komatiites of Muva Supergroup (Seifert et al., 2004). The metabasite horizons are overlapped by a major field of Be-bearing pegmatites and hydrothermal veins that were emplaced during the late stages of the Pan African Orogeny (~530 Ma; John et al., 2004).

Emerald from Sandawana mine (Zimbabwe) (Zwaan et al., 1997) is the result of pegmatite intrusions in the Mweza Greenstone Belt, followed by the injections, along shear zones, of Na-rich and Cr-, Li-, Be- F-, P-, K-, Rb-, Cs-bearing fluids. These fluids caused albitization of the pegmatite and phlogopitization of the wall-rock (Zwaan, 2006). The synkinematic growth of emerald, chromian ilmenorutile, fluorapatite, and holmquistite suggests that emerald formation is closely related to syntectonic K–Na metasomatism, (Zwaan, 2006).

The Be-bearing pegmatite at Kenticha (Ethiopia) is a peraluminous body related to post-accretionary magmatism (Küster, 2009) of I-type or A2-type magmas with either crust derived or hybrid crust–mantle derived magmas. Kenticha (Ethiopia) is a (Sn)-Be-Li-Ta tabular pegmatite. Emerald occurs with lepidolite, spodumene, holmquistite, elbaite, swinfordite, Li-phosphates, amblygonite and lithiophyllite.

2.2 Type-2 deposits

The emerald deposits of Panjshir Valley (Afghanistan) are genetically related to hydrothermal fluid interacting with serpentinite rocks of the suture zone (Groat et al., 2008; Sabot et al., 2000). Emerald occurs in the phlogopite reaction bands (Kazmi and Snee, 1989). The highly saline nature of fluid inclusions in emerald suggests that these deposits have been formed from hydrothermal fluids that interacted with evaporitic sequences (Franz and Morteani, 2002; Giuliani et al., 2005; Giuliani et al., 1997a; Sabot et al., 2000; Vapnik and Moroz, 2000).

Emerald deposits from Colombia are in two narrow bands on both sides of the Cordillera Oriental, and occur in extensional carbonate–silicate–pyrite veins, pockets, and organic-rich black shales of the Early Cretaceous. Emerald occurs in pockets with fluorite, apatite, parisite [$Ca(Ce,La)_2(CO_3)_3F_2$], dolomite and quartz.

The deposits are unusual because there is no evidence for magmatic activity. Several authors reported that emerald crystallized from hydrothermal fluids associated with tectonic activity (Branquet et al., 1999a, 1999b; Cheilletz and Giuliani, 1996; Giuliani et al., 1995; Ottaway et al., 1994). The genetic model of Muzo mine seems to be controlled by the activity of hydrothermal brines which transported evaporitic sulphate to structurally favorable sites. Sulphur generated by thermochemically reduced process reacted with organic matter in the shales to release trapped chromium, vanadium and beryllium, forming emerald (Escobar and Mariano, 1981; Giuliani et al., 2000; Ottaway et al., 1994).

The emerald deposit of Habachtal (Austria) is one of the few emerald sources on the European continent, mined since Roman time and now dormant. The geological context consists of sequence of metapelite and metavolcanic rocks (Habach formation) with interlayered serpentinites, near the contact with the Zentral gneiss. Emerald occurs within metasomatic “blackwall” zones, developed during regional metamorphism. Porphyroblasts of emerald crystallized syn- to post-tectonically, mainly at the contact between muscovite-plagioclase-chlorite boudins and biotite schists.

Geochemical analyses show that the “blackwall” zone is enriched in Be, which suggests a submarine volcanic exhalation source, as pointed out by Grundmann and Morteani (1989). They proposed that the enrichment of Be is due to the destabilization of primary silicate which released Be in the system to form emerald. However, Zwaan (2006) did not agree with this model, while proposing a pegmatite origin for Be, as pegmatite rocks occur in Zentral gneiss. His hypothesis seems also to be confirmed by the high Cs content in Habachtal emerald, about 750 ppm, which excludes an origin from submarine volcanic exhalations that are not generally enriched in Be.

Santa Terezinha deposit is associated with ductile shear zones cutting mafic and ultramafic rocks (Giuliani et al., 1990; Giuliani et al., 1997a, 1997b). Emerald occurs with phlogopite in metasomatized rocks. The talc schists provided sites for thrusting that gave rise to the formation of sheath folds. The absence of granites and related pegmatites, and the low Be concentration in the volcano-sedimentary sequence (<2 ppm) exclude a magmatic origin for Be. However, isotopic data ($\delta^{18}O$ and δD for emerald and coeval phlogopite) are consistent with both magmatic and metamorphic fluids (Groat et al., 2008). A metamorphic origin is therefore proposed for the Santa Terezinha parental fluids. Emerald from Swat Valley (Pakistan) occurs often with fuchsite (Cr-rich muscovite) and Cr-rich green tourmaline in limonitized shear zones within talc-carbonate rocks. It occurs as disseminations or in veins and stockworks, and within fractured quartz-bearing magnesite rocks (Arif et al., 1996; Kazmi et al., 1986). Stable isotopes (Arif et al., 1996) suggest that the mineralization was probably formed by modified hydrothermal solutions derived from an S-type granitic magma.

The most known emerald mines from Egypt occur in a NW-trending band ~45 km along Nugrus Thrust **(**Eastern Desert) (Abdalla and Mohamed, 1999; Harrell, 2004; Grundmann and Giuliani, 2002; Jennings et al., 1993).

The main mineralized centres are Zabara, Sikait, and Urn Kabu. The emerald crystals are commonly restricted to volcano-sedimentary series, dominantly biotite schists, with subordinate amphibolite and serpentinite rocks (Abdalla and Mohamed, 1999). These series are intruded by leucogranite and pegmatite, formed by melting of metapelitic schists (Mohamed and Hasanen, 1997). Mining activity of these deposits probably began toward the end of the 1st century BC, with the pick mining from the late 1st century AD to the 6th century AD (Harrell, 2004).

The best Indian emeralds come from the Rajghar deposit. In 1995 emerald was also discovered embedded in the wall of a well in the village of Sankari Taluka, in the southern Indian state of Tamil Nadu (Panjikar et al., 1997). This emerald, which is all Cr-dominant, occurs in a lenticular belt of micaschist which has been traced for approximately 5 km. According to Panjikar et al. (1997), similarities in physical properties, compositions, and inclusions between the Sankari emerald and those from deposits in Madagascar suggest that the former may have been emplaced into Gondwanaland before India rifted from it.

3 Materials and Analytical Methods

3.1 Materials

Seventeen emerald crystals from different worldwide deposits (Fig. 1) have been analyzed using EMP and SIMS analysis. The size of crystals varies from few millimeters to a centimeter, and their color presents various shades of green.

3.2 Methods

The composition of emerald crystals was determined by electron microprobe analysis using a CAMECA CX 827 (CNR-IGG, Rome) equipped with three wavelength-dispersive spectrometers with automation by Microbeams Services (Victoria, Australia). Accelerating voltage, beam current and diameter were 15 kV, 5-10 μm and 10-20 nA, respectively. Element peaks and background were measured with counting times of 10 s each. Synthetic diopside (SiKα, TAP; CaKα, PET; MgKα, TAP), jadeite (AlKα, TAP; NaKα, TAP), rutile (TiKα, PET), olivine (FeKα, LIF), rhodonite (MnKα, LIF), orthoclase (KKα, PET), and pollucite (CsLα, PET) have been used as standards. Matrix corrections were calculated by the PAP method (Pouchou and Pichoir, 1985), with software supplied by Microbeams Services. The detection limits under the specified working condition vary from 0.05 to 0.1 wt. % with standard deviations from 0.02 to 0.04 wt.%. The analytical error was ~1% rel. for the major elements.

Beryllium, trace- and minor-elements on the study emeralds were done by SIMS with a Cameca IMS 4f ion microprobe installed at CNR-IGG (Pavia) under two separate mass acquisition lists. Be was detected by using a $^{16}O^-$ primary beam of ~1.5 nA current intensity, ~5 μm diameter, accelerated by –12.5 kV. We used the largest contrast diaphragm and field aperture (400- and 1800-μm Ø, respectively), at a mass resolving power of ~ 600 (M/ΔM). The filtered secondary ions (75-125 eV) were extracted and focused under an ion-image field of 25 μm (Ottolini et al., 1993). Beryl crystals no. 13 (blue beryl, Mursinka, Ural Mountains, Russia) and no. 27 (pink beryl, Mujane mine, Zambesia), were used as standards (Aurisicchio et al., 1988). All the other elements were detected proxy to previous SIMS spots on the same crystals, using $^{16}O^-$ primary beam of 10 nA current intensity, focused into a spot of ~15 μm in diameter. We detected signals from the following isotopes ^{7}Li, ^{11}B, ^{45}Sc, ^{47}Ti, ^{51}V, ^{52}Cr, ^{85}Rb, ^{88}Sr, ^{89}Y, ^{90}Zr, ^{93}Nb, ^{133}Cs, ^{138}Ba, ^{232}Th and ^{238}U. All of them were monitored in the same analytical run. $^{45}Sc^+$ and $^{52}Cr^+$ were further corrected for $^{29}Si^{16}O^+$ and $^{24}Mg^{28}Si^+$ interferences at mass 45 and 52, respectively. $^{30}Si^+$ was selected as the isotope of the reference element (Si) for these matrixes. Well-characterized glassy standards among which BB glass and NIST SRM 610 were used to calibrate ion signals (see Ottolini et al., 2004 and ref. therein). Accuracy for Be is estimated to be about 5% rel. and 10% rel. at ppm level for the other elements, except for Rb (15%) and U and Th (20%).

The Principal Component Analysis (PCA) is a statistical method used to explore data, providing information about the relationships among different samples. The application of statistical procedures in the elaboration of chemical results was proposed in the Earth Sciences since ´70s (Davis, 1976; Joreskog et al., 1976;). Recently, the application of PCA has been applied for mapping mineralogical alterations (Moore et al., 2008), characterization of mineral ores (Death et al., 2009), quantification of zinc speciation in soil (Scheinost et al., 2002) and so on. This method has been greatly appreciated in the elaboration of chemical data as it permits to correlate many variables (Baxter and Buck, 2000). Indeed, PCA considers an X data matrix with n rows (samples) and p columns (chemical elements) to create new variables in a lower number respect to the starting data considering only the variables that maximize the difference between samples (Johnson, 1998). The principal components are calculated from X data matrix as orthogonal combinations of the original variables; therefore, the first two or three principal components can describe most of the variance of the system (Baxter, 1999). The score plot is a linear projection of samples onto the first two principal components axes, whereas the loading plot visualizes the correlation between the old variables (chemical elements) and the new PCs.

Here PCA of the covariance matrix was performed using the chemical data resulting by EMPA and SIMS. PCA was performed using XLSTAT® statistical software which runs as an additional component of Microsoft Excel®. Major, minor and trace elements were log10 transformed to avoid deleterious scale effects of clustering results (e.g., V-shaped chemical data; Aruga et al., 1993).

4 Results

In Table 1 are reported the chemical composition of the study emerald (obtained from EMP and SIMS techniques) expressed in oxides, formula and ppm. Most of the samples have Si content ≥ 6 apfu filling their own site T2. Only Australia and Tanzania crystals show T2 site constantly under-saturated by Si. The tetrahedron T1 is almost exclusively occupied by Be, excluding Zimbabwe, Russia and India samples, which have a higher Li content.

The main occupant of the octahedral site is Al, which ranges from 71% to 97% of the total site occupancy. Mg, Fe and Cr ions are the main substitutes for Al, usually in the order Mg>Fe>Cr, except for Nigeria Jos samples where Fe is higher than Mg and Cr. Moreover, emeralds from most Type-2 deposits (Afghanistan, Colombia, Egypt, Pakistan) and Zimbabwe deposit (Type-1) have a Cr content higher than Fe. Indeed, despite of the intense green color of the sample set, Cr content ranges from 0 to 0.183 apfu (Table 1).

Sodium is the predominant cation in the channels and its content is mainly controlled by the octahedral site substitutions. Channel occupancy varies from 0.400 apfu for both Types-1 and 2 (e.g. Brazil and Zimbabwe, respectively) to lower values that are most typical for Type-1 deposits (e.g., Tanzania, 0.027 apfu).

Figure 2, displaying the expected inverse relationship between Al (Y-site) and its substituents, highlights a trend growing along the line defined by Al (Y-site) = 2 apfu to ∑ substituents = 1 apfu. Samples from Nigeria and Tanzania with Al next to 2 apfu, and Brazil, Pakistan and Egypt El Zabarà next to 1.4 apfu represent the ends of this trend. The ternary diagram of Figure 3 shows the distribution of three oxides (MgO, FeO and Cr_2O_3) substituting for Al_2O_3 confirming the clustering of emerald samples around MgO corner. However, the Nigeria and Tanzania deposits show a strong predominance of FeO (Nigeria) followed by Tanzania (one value at ~ 50% of Cr_2O_3); emerald from Pakistan contains about 25% Cr_2O_3 and FeO.

Figure 4 displays the linear correlation between channel charge (ΣX-site) and divalent Mg+Fe+Mn substituents for Al. Data lying to the left of the 1:1 line from both Type-1 (Madagascar, Russia, Tanzania and Zimbabwe) and Type-2 (Austria and Ethiopia) deposits indicate that some Fe in emerald is present as Fe^{3+}, whereas the lack of data on the right side suggests that the substitution of Li^+ for Be^{2+} is very limited.

Figure 5, showing the ΣX-site versus Li content (apfu) confirms the low Li^+ for Be^{2+} substitution. Among Type-1 deposits, only Zimbabwe samples reach 0.08 Li apfu, whereas the lowest contents are shown by Tanzania and Nigeria. Australia and Russia show intermediate values of both ΣX and Li. Colombia and Afghanistan (Type-2) are moderately enriched in ΣX but show a very low Li content. All the other emerald crystals of both type deposits are gathered in an area characterized by higher channel content and Li varying from near zero (Brazil, Egypt, Mozambique, and Madagascar) towards intermediate values, about 0.04 apfu (Austria, Pakistan, India, Ethiopia, Zambia).

The systematic variation of trace elements in emerald from different sites is illustrated in the C1-chondrite normalized (Anders and Grevesse, 1989**)** spider diagrams of Fig. 6a (Type-1) and Fig. 6b (Type-2). These diagrams include Light (LE: Li, B, Na), Large Ion Lithofile (LILE: Rb, Ba, K, Sr, Cs), High Field Strength (HFSE: Th, U, Nb, Zr, Ti) and Chromophore Transition (CTE: Sc, V, Cr) Elements. Additional binary diagrams, LILE vs CTE (Fig. 7), Cr vs V (Fig. 8), Rb vs Cs (Fig. 9), and Li vs B (Fig. 10) and LILE vs HFSE (Fig.11) were considered to highlight peculiar differences inside the emerald deposits.

LE and LILE patterns (Fig. 6a, 6b) of all samples display the highest enrichments in Li, Na, and Cs, followed by Rb and, to a lesser extent, K. The highest values of Rb and K concern emerald crystals from Type-1 deposits. All samples are normally depleted in Sr, Ba and B. LE and LILE display a wide range of concentration, excluding Ba and Sr. In more detail (see binary diagrams of Figs. 9, 10) Colombia shows the lowest contents of B and Rb, whereas Zimbabwe is

enriched in Li, Rb and Cs. High contents of Rb and, the highest contents of the whole LILE (Fig.11) characterize Mozambique and Madagascar deposits, whereas the deposit of S. Terezinha (Brazil) is characterized by the highest Cs content followed by samples from Zimbabwe and Ethiopia.

Within HFSE (Fig. 6a, 6b), U displays the highest and most homogeneous concentrations for both Type deposits, followed by Th. The others, Nb, Zr, Ti and Y display very low concentrations and scattered behavior. However, as shown in Fig. 11, Zimbabwe (Type-1) and Egypt El Zabara (Type-2) display the highest contents of HFSE.

Concerning the CTE (Fig. 6a, 6b), Cr, V and Sc show relatively high concentrations, roughly in the order Cr>Sc>V of which the latter two elements reach higher values in Type-2 deposits. Emerald from Tanzania and Mozambique deposits (Type-1) display the lowest Sc and among the lowest V contents; Pakistan and Colombia crystals (Type-2) are characterized by the highest CTE contents (Fig. 7). Moreover, as evidenced by the binary diagram of Fig. 8, Pakistan has the highest Cr and among the lowest V contents, whereas Colombia presents the highest V and among the lowest Cr contents.

PCA investigation was performed on the chemical data to identify possible distinct groups for provenance purposes (Fig 12I, 12II, 12III). The first elaboration hereafter named “discriminant data I” (Fig. 12I) include EMPA data for SiO_2, Al_2O_3, FeO, MnO, MgO, CaO, Na_2O and K_2O, and SIMS data for Be, Li Cr, V, Ti and Cs of (Table 1). This plot shows that samples from Nigeria and Tanzania deposits are grouped together for their high Al_2O_3 content. Emerald from Afghanistan, Colombia, Russia and Australia is also characterized by high Al_2O_3 content; however, they are further distinguished in two distinct groups by the content of SiO_2 and BeO (Afghanistan and Colombia), and the low content of CaO, MnO and K_2O (Russia and Australia). Crystals from Madagascar and Mozambique are Ca-rich and show high content of K_2O. Samples from Zimbabwe are characterized by high amount of Li, whereas samples from Zambia display the lowest content of SiO_2. The other districts (Austria, Brazil, Egypt, Ethiopia, India, and Pakistan) are plotted in the same area of the score plot suggesting that none of the considered elements can separate them into distinctive groups.

The second elaboration (Fig. 12II) includes the elements used for the previous plot and the remaining traces measured by SIMS (in ppm, at the bottom of Table 1). This plot, here on named “discriminant data II” shows that emeralds from Nigeria, Tanzania, Afghanistan, Colombia, Russia and Australia fall on the right part of the diagram basing on the Al_2O_3 content. Nigeria and Tanzania are plotted together by their highest values of Al. Colombian and Afghanistan samples are discriminated by the high SiO_2 content; however, they are more separated by the influence of V (Colombia) and Sc content (Afghanistan). Zambian samples are separated by the lowest content of SiO_2 and the

higher content of B. Other districts, i.e. Austria, Pakistan, India, Brazil, Egypt, Ethiopia, Mozambique, Madagascar and Zimbabwe are plotted in the same group, even if the latter is slightly separated by the influence of Li content.

Finally, the loading plot of Fig. 12III, hereafter named “discriminant data III” included all the elements analyzed by SIMS (except Be). It shows that emeralds from Colombia are clearly distinguished based on the high content of V, and those from Pakistan are separated by their content of Cr. Moreover, the very low content of LILE allows separating Sumbawanga (Tanzania) and Jos (Nigeria) samples which in Fig. 12 I,II fall in the same cluster.

5 Discussion and conclusion

The emerald crystals here considered are largely coincident with those included in the classification schemes proposed by Schwarz and Giuliani (2001) and Schwarz et al. (2001); in addition, samples from Alto Ligonha (Mozambique) and Sumbawanga (Tanzania) are also reported.

PCA plots of Figs. 12 I,II,III allow to discriminate for Type-1 deposits five different clusters; two clusters include one deposit (Zambia, Zimbabwe), whereas three clusters include two deposits (Australia and Russia; Madagascar and Mozambique; Nigeria and Tanzania). The emerald from Ethiopia, classified as Type-1 (in Geological background of emerald deposits section) presents contrasting behavior when PCA treatment is considered. In detail, in Figs. 12I and III the data plot **i**n the indiscriminate cluster of Type-2 emerald; whereas, in Fig. 12II they plot close to the cluster including Type-1 Madagascar and Mozambique deposits.

Within Type-2 deposits, only Afghanistan and Colombia form a distinct cluster, whereas all the others deposit plot in the same group.

5.1 Type-1 deposits

Concerning the deposits of Malyshevsk-Poona (Russia and Australia), the chemical composition highlighted that these samples are Al-rich and depleted in Ca, Cr and Mn. These emerald crystals formed from metasomatic fluids having similar features, even if originated in different geological contexts, as testified by the occurrence of analogous paragenetic assemblage. The emerald of Poona is the results of metamorphic reactions between preexisting greisen and basic-ultrabasic rocks. On the contrary, Malyshevsk deposit occurs into desilicified pegmatites. Both mineralizing fluids presented an enrichment of Al, and a loss of Ca, Mn, and Cr. However, the emerald of Russia Malyshevsk presents higher content of Li (Fig. 5; Fig. 8) than those of Poona. This is likely related to fluids probably originating from LCT pegmatite melts.

The cluster including both Madagascar and Mozambique samples is related to their high and similar content of Ca, Rb and K (see also Figs. 6a, 7 and 9). However, a possible discrimination between these two deposits is linked to the higher content of Cr and to a certain predominance of CTE in emeralds from Madagascar (Figs. 6 and 8) and LILE in Mozambique (Fig. 7**)**.

The highest content of Al and Fe (Fig. 12 I, II; Fig. 3) that characterize emerald from Sumbawanga (Tanzania), and Jos (Nigeria), suggest that also mine of Subawanga, not reported in the considered classification scheme (Schwarz and Giuliani, 2001; Schwarz et al., 2001), can be included in the sub group of Type 1 pegmatites, i.e. pegmatites without schist at contact zone. Diagram of Fig. 3 also helps to discriminate the two districts based on the highest iron content (>75%) of Jos mine and the highest Cr content (from 15 to 50%) of Sumbawanga (Tanzania) crystal. Moreover, the lower content of Zr, Sc, Cs and V, and the higher content of Cr, V and K distinguish Tanzania from Nigeria emerald (Figs. 6, 8 and 9).

Within the remaining Type-1 districts forming single cluster by the PCA, emerald from Zambia is characterized by the lowest values of silica and higher B contents, whereas that from Zimbabwe presents a content of LILE, particularly Li and Rb, higher than that of Zambia (Fig. 6a, 9 and 10).

The Ethiopian is the only Type-1 emerald that fall in the not discriminated PCA cluster (Fig. 12I-II-III). It is characterized by high Li and Cs contents, reflecting a contribution of pegmatite fluid in the emerald formation (Küster, 2009). The samples of indiscriminate cluster present few geochemical markers that could help for provenance purpose. For this reason, emerald from those deposits can be better discriminated using isotopic data of oxygen reported by Giuliani (2000) and those reported in Table S1 (supplementary material). Indeed, the signature of Ethiopian emerald is $\delta^{18}O \sim 8‰$, which is different from that of Habactal ($\delta^{18}O \sim 6.8‰$) and those of the others Type-2 districts, which have values of $\delta^{18}O \geq 10‰$.

5.2 Type-2 deposits

Type-2 group includes deposits located in Afghanistan (Panjshir Valley), Austria (Habactal), Brazil (Santa Terezinha), Pakistan (Swat Valley), Egypt (Eastern desert) and Colombia (Mouzo), which are controlled by tectonic events.

Based on results from PCA analysis (Figs. 12I and 12II) Afghan and Colombian emeralds are distinguished for their high content of Si and Al. However, the emerald of these two deposits differs for the LILE, LE and CTE contents (Figs. 6b and 7). These latter are fundamental to discriminate the two deposits as Afghan emerald is enriched in Sc (about 1000 ppm) and the Colombian emerald are the richest in V (about 4000 ppm) (Fig. 8 and Fig. 12III). These features are

related to the different reservoirs involved in their genesis. In more detail, the hydrothermal fluids in Afghanistan leached Cr and Sc from basic/ultrabasic rocks, whereas the mineralizing fluids intercepted vanadate-bearing black-shale (Franz and Morteani, 2002; Giuliani et al., 1997a; Giuliani et al., 2005; Sabot et al., 2000; Vapnik and Moroz, 2000). The other deposits are clustered all together and PCA elaborations are not useful to identify peculiar geochemical fingerprints for provenance purposes.

Egyptian samples are characterized by high content of Mg, Fe, CTE and low LILE. They are clustered together in statistical elaboration. However, samples from El-Zabara can easily distinguish from those of El-Sikait for the higher content of B (Fig. 10) and HFSE (Fig. 11). The high value of boron suggests a contribution of leucogranite fluids, outcropping in the area (Mohamed and Hasanen, 1997).

"Discriminant data III" plot (Fig.12III) and Fig. 8 allow distinguishing emeralds from Pakistan for the highest Cr content. Emerald from Pakistan (Swat Valley) is characterized by low content of Al and LILE, whereas the content of CTE along with Mg and Fe is very high, highlighting an interaction between mineralizing fluids and limonitized rocks as well as magnesite (Groat et al., 2008).

The analysis of traces elements and the comparison of spider diagrams highlight that emeralds from Austria have the lowest content of CTE and LILE (Fig. 7). The emerald from Habachtal does not present specific feature respect to the others, however its high content of Mg along with that of Be suggest an interaction between pegmatite fluids and serpentine rocks, even if pegmatite bodies does not outcrop in the area as previously quoted by Zwann (2006).

The key features of emerald from Santa Terezinha are the highest content of Mg and LILE respect to emerald from other deposits. CTE content is also high. Some authors (Groat et al., 2008) report that the source of Be is not magmatic. However, the highest content of Cs (Figs. 6b and 9) seems to support the hypothesis that also magmatic fluids could be mixed with those of metamorphic origin from which emerald crystallized. Emerald from India is Li-Cs enriched with a moderate content of Mg and Cr, suggesting that they formed from magmatic/pegmatite fluids which leached Mg and Cr from basic/ultrabasic rocks in Gondwanaland.

We have reported, for the first time both major and trace elements of emeralds from several worldwide deposits. Binary, ternary and PCA diagrams of major, minor and trace elements enable to identify geochemical markers which help to discriminate emeralds from various sources. The data treatment along with the genetic models of emerald formation represents an important archive for reconstructing the environment of the emerald, resulting useful for provenance purposes. In detail, the emerald related to granitic intrusions (Type-1) or in environments controlled by tectonic event

(Type-2) can be distinguished on the basis of their major and trace element concentrations, which are the result of the complex metasomatic fluids that give rise to emerald crystallization.

Acknowledgments

This research was financed by the Consiglio Nazionale delle Ricerche-Istituto di Geoscienze e Georisorse and Sapienza Università di Roma, Italy. Authors are indebted to Dr. I Moroz for generously providing chemical data of some samples.

References

Abdalla, H.M., Mohamed, F.H., 1999. Mineralogical and geochemical investigation of emerald and beryl mineralization. Pan-African belt of Egypt: genetic and exploration aspects. J. Afr. Earth Sci. 28, 581-598.

Anders, E., Grevesse, N., 1989. Abundances of the elements-Meteoritic and solar. Geochim. Cosmochim. Acta 53, 197-214.

Aruga, R., Mirti, P., Casoli, A. 1993. Application of multivariate chemometric techniques to the study of Roman pottery (terra sigillata). Anal. Chem. Acta 276, 197-204.

Aurisicchio, C., Fioravanti, G., Grubessi, O., Zanazzi, P.F., 1988. Reappraisal of the crystal chemistry of beryl. Am. Mineral. 73, 826-837.

Aurisicchio, C., Ottolini, L., De Vito, C., 2007. Tracing the archaeological emerald origin by EMPA and SIMS data. Gemmological Conference (IGC 2007) Moscow Russia 15-19 July Abstracts Volume 8-9.

Arif, M., Fallick, A.E., Moon, A.E. 1996. The genesis of emeralds and their host rocks from Swat northwestern Pakistan: a stable-isotope investigation. Miner. Deposita 31, 255-268.

Artioli, G., Rinaldi, R., Ståhl, K., Zanazzi, P.F., 1993. Structure refinements of beryl by single-crystal neutron and X-ray diffraction. Am. Mineral. 78, 762-768.

Barton, M.D., Young, S., 2002. Non-pegmatitic deposits of beryllium: mineralogy geology phase equilibria and origin Reviews in Mineralogy and Geochemistry 50, 591-691.

Baxter, M.J., 1999. Detecting multivariate outliers in artefact compositional data. Archaeometry 41, 321-338.

Baxter, M.J., Buck, C.E. 2000. Data handling and statistical analysis, in: Ciliberto, E., Spoto, G. (Eds.), Modern analytical methods in art and archaeology. John Willey, New York, pp. 681-746.

Branquet, Y., Laumonier, B., Cheilletz, A., Giuliani, G. 1999a. Emeralds in the Eastern Cordillera of Colombia: two tectonic settings for one mineralization. Geology 27, 597-600.

Branquet, Y., Cheilletz, A., Giuliani, G., Laumonier, B., 1999b. Fluidized hydrothermal breccia in dilatant faults during thrusting: the Colombian emerald deposits, in: McCaffrey, K.J.W., Lonergan, L., Wilkinson, J.J. (Eds.), Fractures Fluid Flow and Mineralization 155. Geological Society of London, pp. 183-19.

Chielletz, A., Giuliani, G., 1996. The genesis of Colombian emeralds: a restatement. Miner. Deposita 31, 359-364.

Cronwright, M.S., 2005. A review of the rare-element pegmatites of the Alto Ligonha Pegmatite Province northern Mozambique and exploration guidelines. MSc Dissertation. Rhodes University Grahamstown South Africa.

Davis, J., 1976. Statistics and Data Analysis in Geology. Wiley, New York.

Death, D.L., Cunningham, A.P., Pollard, L.J., 2009. Multi-element and mineralogical analysis of mineral ores using laser induced breakdown spectroscopy and chemometric analysis. Spectrochim. Acta B 64, 1048-1058.

Dill, H.G., 2015. Pegmatites and aplites: Their genetic and applied ore geology. Ore Geol. Rev. 69, 417-561.

Dereppe, J.M., Moreaux, C., Chauvaux, B., Schwarz, D., 2000. Classification of emeralds by artificial neural networks. J. Gemmol. 27, 93-105.

Dias, M.B., Wilson, W.E., 2000. The Alto Ligonha pegmatites: Mozambique. Mineral. Rec. 31, 459-497.

Escobar, R., Mariano, A.N., 1981. On the origin of the Colombian emeralds. Nuclide Spectra XIV, 1025-1081.

Fersman, A.E., 1929. Geochemische Migration der Elemente. Abh. Prakt. Geologie Bergwirtschaftlehre 18, 74-116.

Franz, G., Morteani, G., 2002. Be-minerals: synthesis stability and occurrence in metamorphic rocks, in: Grew, E.S. (Ed.), Beryllium: Mineralogy Petrology and Geochemistry. Reviews in Mineralogy and Geochemistry 50, 551-589.

Gavrilenko, E.V., 2003. Esmeraldas de los Urales (Rusia): condiciones de formacion y caracterizacion comparativa con las esmeraldas de otros origenes. Unpublished M Sc thesis Universidad Politécnica de Madrid, Spain.

Gavrilenko, E.V., Dashevsky, D.M., 1998. Properties of emeralds of different genesis and their diagnostic meaning. Proceedings of the Russian Mineralogical Society 127, 45-57.

Giuliani, G., Silva, L.J.H.D., Couto, P., 1990. Origin of emerald deposits of Brazil. Miner. Deposita 25. 57-64.

Giuliani, G., Cheilletz, A., Arboleda, C., Carrillo, V., Rueda, F., Baker, J.H., 1995. An evaporitic origin of the parent brines of Colombian emeralds: fluid inclusion and sulphur isotope evidence. Eur. J. Mineral. 7, 151-165.

Giuliani, G., France-Lanord, C., Zimmermann, J.L., Cheilletz, A., Arboleda, C., Charoy, B., Coget, P., Fontan, F., Giard, D., 1997a. Fluid composition and δD of channel H_2O and $\delta^{18}O$ of lattice oxygen in beryls: genetic implications for Brazilian Colombian and Afghanistan emerald deposits. Intern. Geol. Rev. 39, 400-424.

Giuliani, G., Cheilletz, A., Zimmermann, J.L., Ribeiro-Althoff, A.M., France-Lanord, C., Feraud, G., 1997b. Les gisements d'émeraude du Brésil: genèse et typologie. Chronique de la Recherche Minière 526, 17-61.

Giuliani, G., Christian, F., Cheilletz, A., Coget, P., Branquet, Y., Laumomnier, B., 2000. Sulfate reduction by organic matter in Colombian emerald deposits: chemical and stable isotope (C O H) evidence. Econ. Geol. 95, 1129-1153.

Giuliani, G., Marty, B., Banks, D., 2005. Noble gases in fluid inclusions from emeralds: implications for the origin of fluids and constraints on fluid-rock interactions. Proceedings XVIII European current research on fluid inclusions (ECROFI).

Groat, L.A., Giuliani, G., Marshall, D.D., Turner, D., 2008. Emerald deposits and occurrences: A review. Ore Geol Rev. 34, 87-112.

Grundmann, G., Morteani, G., 1989. Emerald mineralization during regional metamorphism: the Habachtal (Austria) and Leydsdorp (Transvaal South Africa) deposits. Econ. Geol. 84, 1835-1849.

Grundmann, G., Morteani, G., 1995. Australia Ein neues Vorkommen von Smaragd Alexandrit Rubin und Saphir in einem Topas-fuehrenden Phlogopit-Fels von Poona Cue District West-Australien. Zeitschrift der Deutschen Gemmologischen Gesellschaft 44, 11-29.

Grundmann, G., Giuliani, G., 2002. Emeralds of the world. Extra Lapis English 2, 24-35.

Hammarstrom, J.M., 1989. Mineral chemistry of emeralds and some minerals from Pakistan and Afghanistan: an electron microprobe study, in: Kazmi, A.H., Snee, I.W. (Eds.), Emeralds of Pakistan. Van Nostrand Reinhold, New York, pp. 125-150

Harrell, J.A., 2004. Archaeological geology of the world's first emerald mine. Geosc. Canada 31, 69-76.

Joreskog, K., Klovan, J., Rayment, R. 1976. Geological Factor Analysis. Elsevier Scientific Publishing Company, New York.

Jennings, R.H., Kammerling, R.C., Kovaltchouk, A., Calederon, G.P., El Baz, M.K., Koivula, J.I., 1993. Emeralds and green beryls of upper Egypt. Gems Gemol. 29, 100-115.

John, T., Schenk, V., Mezger, K., Tembo, F., 2004. Timing and PT evolution of white schist metamorphism in the Lufilian Arc-Zambezi Belt Orogen (Zambia): implications for the assembly of Gondwana. J. Geol. 112, 71-90.

Johnson, D.E., 1998. Applied multivariate methods for data analysts, Duxbury Press, Pacific Grove.

Kazmi, A.H., Snee, L.W., 1989. Geology of the world emerald deposits: a brief review, in: Kazmi, A.H., Snee, L.W. (Eds.), Emeralds of Pakistan. Van Nostrand Reinhold, New York, pp. 165-228.

Kazmi, A.H., Lawrence, R.D., Anwar, J., Snee, L.W., Hussain, S., 1986. Mingora emerald deposits (Pakistan): suture-associated gem mineralization. Econ. Geol. 81, 2022-2028.

Kupriyanova, I.I., 2002. On the genesis of the Malyshevsk beryllium-emerald deposit (Middle Urals Russia). Geol. Ore Deposits 44, 276-290.

Küster, D., 2009. Granitoid-hosted Ta mineralization in the Arabian–Nubian Shield: ore deposit types tectono-metallogenetic setting and petrogenetic framework. Ore Geol. Rev. 35, 68-86.

McManus, C.E., De Lucia, F., Harmon, R., McMillan, N.J., Whitmore, R. 2004. Trace element concentrations of pegmatite gems: tracers of petrogenesis and terrorist funding. Geol. Soc. Am., Abstr. with Programs 36, 226.

Mohamed, F.H., Hasanen, M.A., 1997. Geochemistry and petrogenesis of Sikait leucogranite Egypt: an example of S-type granite in a metapelitic sequence. Geologische Rundschau 86, 81-92.

Moine, B., Chan Peng, C., Mercier, A., 2004. Rôle du fluor dans la formation des gisements d'émeraude de Mananjary (Est de Madagascar). Comptes Rendus Geoscience 336, 513-522.

Moore, F., Rastmanesh, F., Asadi, H., Modabberi, S. 2008. Mapping mineralogical alteration using principal-component analysis and matched filter processing in the Takab area north-west Iran from ASTER data. Intern. J. Remote Sensing 29, 2851-2867.

Moroz, I,. Vapnik, Y., Eliezri, I., Roth, M., 2001. Mineral and fluid inclusion study of emeralds from the Lake Manyara and Sumbawanga deposits. J. African Earth Sci. 33, 377-390.

Mumme, I., 1982. The Emerald: Its Occurrence Discrimination and Valuation. Mumme Publications, New South Wales.

Ottaway, T.L., Wicks, F.J., Bryndzia, L.T., Keyser, T.K., Spooner, E.T.C., 1994. Formation of the Muzo hydrothermal emerald deposit in Colombia. Nature 369, 552–554.

Ottolini, L., Bottazzi, P., Vannucci, R., 1993. Quantification of lithium beryllium and boron in silicates by Secondary Ion Mass Spectrometry using Conventional Energy Filtering. Anal. Chemistry 65, 1960-1968.

Ottolini, L., Camara, F., Devouard, B., 2004. New SIMS procedures for the Characterization of a Complex Silicate Matrix $Na_3(REEThCaU)Si_6O_{15}\cdot 25H_2O$ (Sazhinite) and Comparison with EMPA and SREF Results. Microchim. Acta 145, 139-146.

Panjikar, J., Ramchandran, K.T., Balu, K., 1997. New emerald deposits from southern India. Australian Gemmologist 19, 427-432.

Pekov, I., 1998. Minerals First discovered on the territory of the former Soviet Union, Ocean Pictures, Moscow.

Pouchou, J.L., Pichoir, F., 1985. "PAP" f(rZ) procedure for improved quantitative microanalysis, in: Armstrong, J.T. (Ed.), Microbeam Analysis. San Francisco Press, San Francisco California, pp. 104-106.

Sabot, B., Cheilletz, A., de Donato, P., Banks, D., Levresse, G., Barrès, O., 2000. Afghan emeralds face Colombian cousins. Chronique de la Recherche Minière 541, 111-114.

Scheinost, A.C., Kretzschmar, R., Pfister, S., Roberts, D.R., 2002. Combining selective sequential extractions X-ray absorption spectroscopy and principal component analysis for quantitative zinc speciation. Soil Environmental Science and Technology 36, 5021-5028.

Schmidt, W., 1986. Geologische Entwicklung und Lagerstättenbildung der Pegmatitregion von Alto Ligonha VR Moçambique. Dissertation B Mining Academy, Freiberg.

Schwarz, D., Giuliani, G., 2001. Emerald deposits-a review. Australian Gemmologist 21, 17-23.

Schwarz, D., Kanis, J., Kinnaird, J., 1996. Emerald and green beryl from central Nigeria. J. Gemmology 25, 117-141.

Schwarz, D., Giuliani, G., Grundmann, G., Glas, M., 2001. Die Entstehung der Smaragde ein vieldisskutiertes Thema, in: Schwarz, D., Hochlitner, R. (Eds.), Smaragde der kostbarste Beryll, der teuerste Edelstein (ExtraLapis), Weis, pp. 68-73.

Seifert, A.V., Žáček, V., Vrána, S., Pecina, V., Zachariáš, J., Zwaan, J.C., 2004. Emerald Mineralization in the Kafubu area Zambia. Bull. Geosc. 79, 1-40.

Themelis, T., 1989. Gemmology; new east African deposits. Lapidary Journal 42, 34-37.

Thomas, R., Davidson, P., 2010. Hambergite-rich melt inclusions in morganite crystals from the Muiane pegmatite Mozambique and some remarks on the paragenesis of hambergite. Mineral. Petrol. 100, 227-23.

Vapnik, Y.E., Moroz, I., 2000. Fluid inclusions in emerald from the Jos Complex (central Nigeria). Schweizerische Mineralogische und Petrographische Mitteilungen 80, 117-129.

Zwaan, J.C. 2006. Gemmology geology and origin of the Sandawana emerald deposits Zimbabwe. Scripta Geologica 131, 1-211.

Zwaan, J.C., Kanis, J., Petsch, E.J., 1997. Update on emeralds from the Sandawana mines Zimbabwe. Gems and Gemol. 33, 80-100.

Figure and Table captions

Fig. 1 A sketch map of the location of the emerald mines.

Fig. 2 Al (Y-site) versus the sum of its substituents in atoms per formula unit in studied emerald.

Fig. 3 Distribution of MgO, FeO and Cr_2O_3 of studied emerald (from Hammarstrom 1989). Symbols as in Fig. 2.

Fig. 4 Sum of divalent octahedral cations versus sum of channel cations of the studied crystals. Symbols as in Fig. 2.

Fig. 5 Li occupancy in tetrahedral (T1) site versus channel occupancy in atoms per formula unit in studied emerald. Symbols as in Fig. 2.

Fig. 6 C1-chondrite normalized (Anders and Grevesse, 1989**)** multi-element distribution diagrams in studied crystals distinguished in Type-1 (a) and Type-2 (b) emerald related to their genetic model of formation (Schwarz and Giuliani 2001). The element concentrations are expressed in ppm. Symbols as in Fig. 2.

Fig. 7 Transitional chromophore element versus large ion lithofile element concentrations (expressed in ppm) of studied samples. Symbols as in Fig. 2. The boxes highlighted the most discriminated crystals.

Fig. 8 Cromium versus vanadium concentrations (expressed in ppm) of studied samples. Symbols as in Fig. 2. The boxes highlighted the most discriminated crystals.

Fig. 9 Rubidium versus cesium concentrations (expressed in ppm) of studied samples. Symbols as in Fig. 2. The boxes highlighted the most discriminated crystals.

Fig. 10 Boron versus litium concentrations (expressed in ppm) of studied samples. Symbols as in Fig. 2. The boxes highlighted the most discriminated crystals.

Fig. 11 Hight field strength versus large ion lithofile elements concentrations (expressed in ppm) of studied samples. Symbols as in Fig. 2. The boxes highlighted the most discriminated crystals.

Fig. 12a PCA analysis of Discriminant data 1 (see text) was performed using EMP data for SiO_2 Al_2O_3 FeO MnO MgO CaO Na_2O and K_2O and SIMS data for Be Li Cr V Ti and Cs.

Fig. 12b PCA analysis of Discriminant data 2 (see text) was performed using EMP data for SiO_2 Al_2O_3 FeO MnO MgO CaO Na_2O and K_2O and SIMS data for Be Li and all the trace elements reported in Table 1.

Fig. 12c PCA analysis of Discriminant data 3 (see text) was performed using all SIMS data excluding Be (Table 1).

Table 1 Chemical composition of study emerald distinguished in Type-1 (a) and Type-2 (b) according to their genetic model of formation (Schwarz and Giuliani, 2001). Number of atoms (atomic fraction) calculated on the basis of 18 oxygens. nd = not determined; apfu = atoms per formula units.


Russia
Austria
Afghanistan
Pakistan
India
Egypt
Nigeria
Ethiopia
Brazil
Tanzania
Colombia
Zambia
Mozambique
Zimbabwe
Madagascar
Australia (Pool)

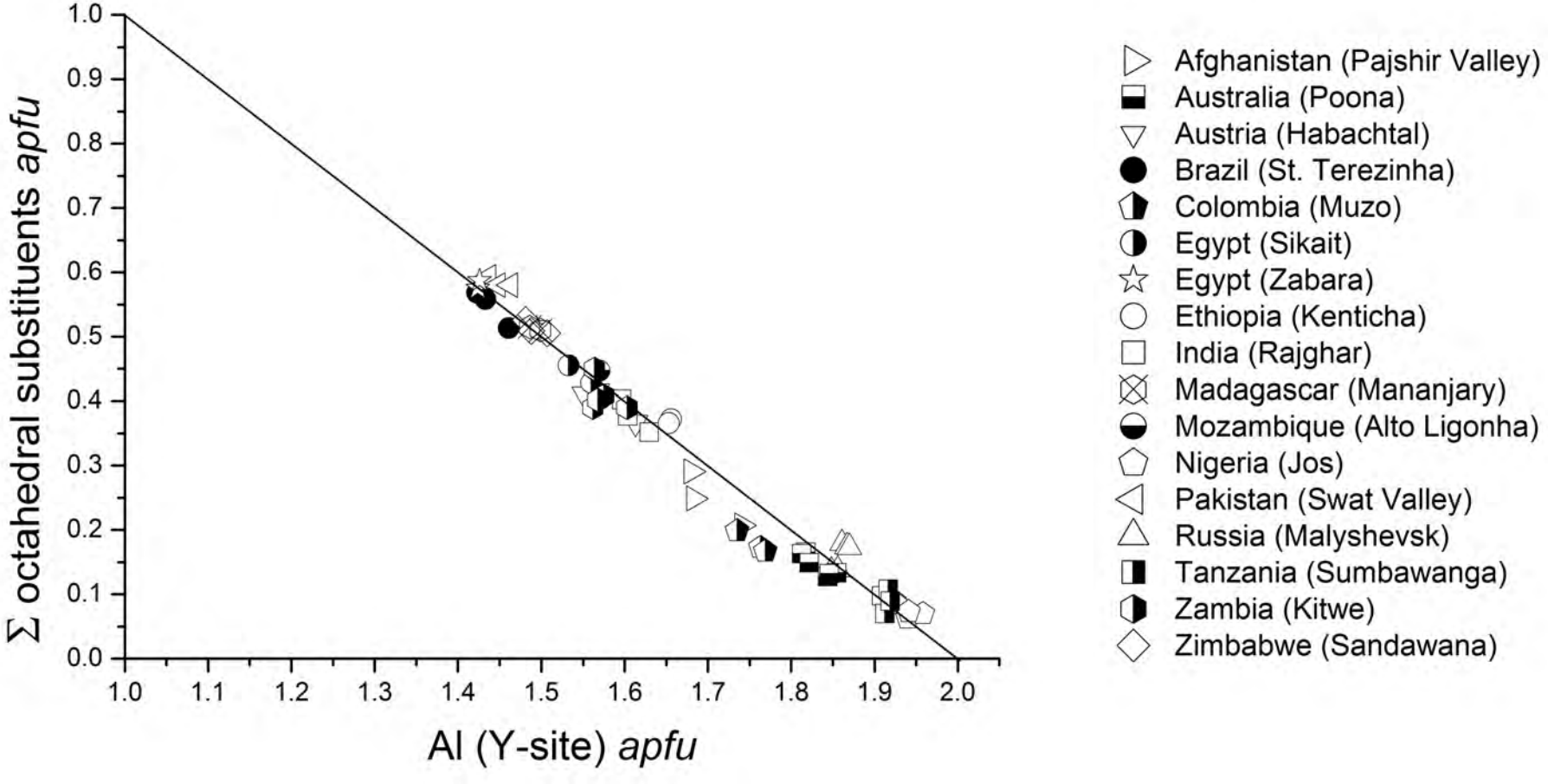
Σ octahedral substituents *apfu*
Al (Y-site) *apfu*
1.0
0.9
0.8
0.7
0.6
0.5
0.4
0.3
0.2
0.1
0.0
1.0
1.1
1.2
1.3
1.4
1.5
1.6
1.7
1.8
1.9
2.0
Afghanistan (Pajshir Valley)
Australia (Poona)
Austria (Habachtal)
Brazil (St. Terezinha)
Colombia (Muzo)
Egypt (Sikait)
Egypt (Zabara)
Ethiopia (Kenticha)
India (Rajghar)
Madagascar (Mananjary)
Mozambique (Alto Ligonha)
Nigeria (Jos)
Pakistan (Swat Valley)
Russia (Malyshevsk)
Tanzania (Sumbawanga)
Zambia (Kitwe)
Zimbabwe (Sandawana)

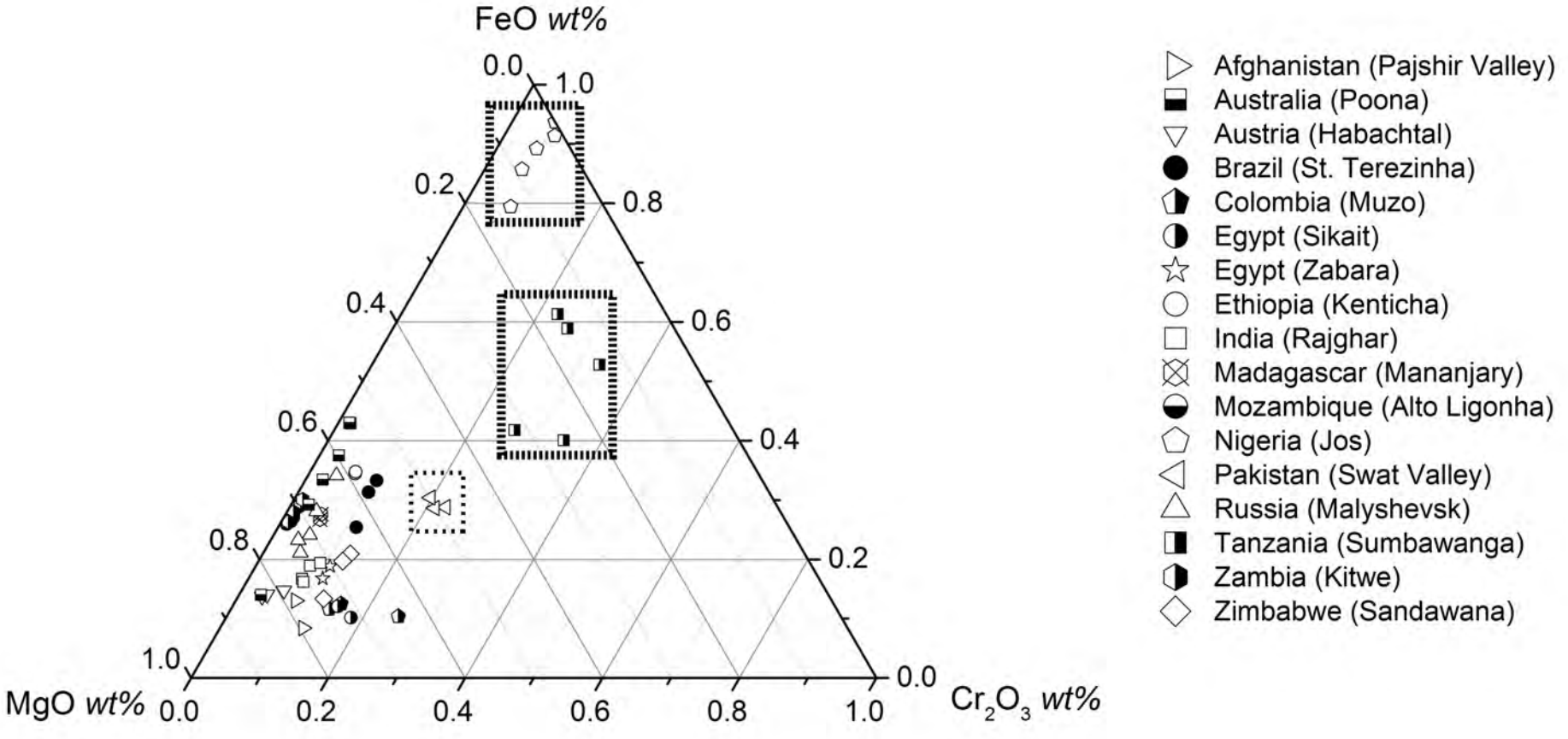
FeO wt%
0.0
1.0
0.2
0.8
0.4
0.6
0.6
0.4
0.8
0.2
1.0
0.0
MgO wt%
0.0
0.2
0.4
0.6
0.8
1.0
Cr2O3 wt%
Afghanistan (Pajshir Valley)
Australia (Poona)
Austria (Habachtal)
Brazil (St. Terezinha)
Colombia (Muzo)
Egypt (Sikait)
Egypt (Zabara)
Ethiopia (Kenticha)
India (Rajghar)
Madagascar (Mananjary)
Mozambique (Alto Ligonha)
Nigeria (Jos)
Pakistan (Swat Valley)
Russia (Malyshevsk)
Tanzania (Sumbawanga)
Zambia (Kitwe)
Zimbabwe (Sandawana)

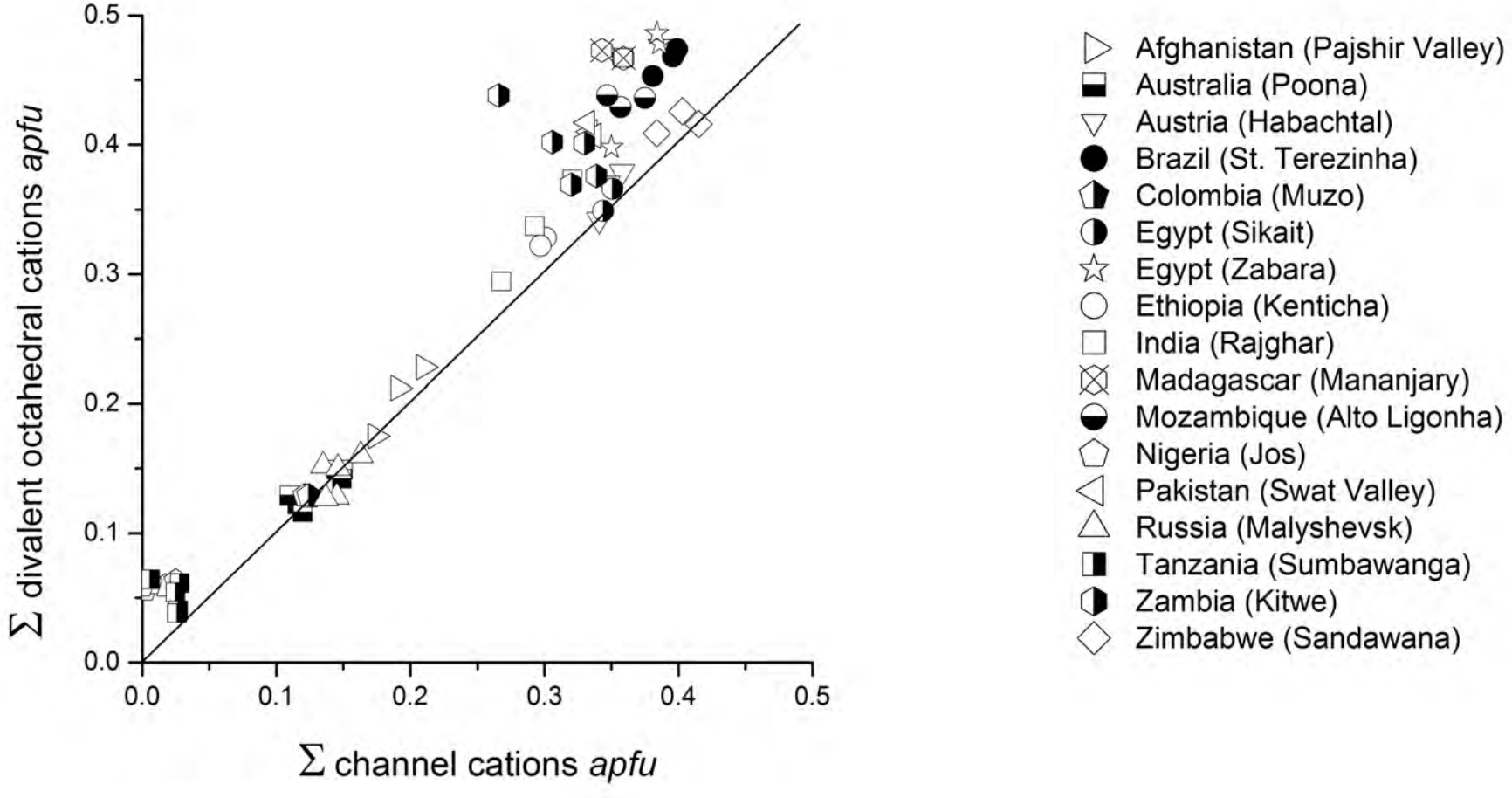
0.5
0.4
0.3
0.2
0.1
0.0
0.0
0.1
0.2
0.3
0.4
0.5
Σ divalent octahedral cations apfu
Σ channel cations apfu
Afghanistan (Pajshir Valley)
Australia (Poona)
Austria (Habachtal)
Brazil (St. Terezinha)
Colombia (Muzo)
Egypt (Sikait)
Egypt (Zabara)
Ethiopia (Kenticha)
India (Rajghar)
Madagascar (Mananjary)
Mozambique (Alto Ligonha)
Nigeria (Jos)
Pakistan (Swat Valley)
Russia (Malyshevsk)
Tanzania (Sumbawanga)
Zambia (Kitwe)
Zimbabwe (Sandawana)

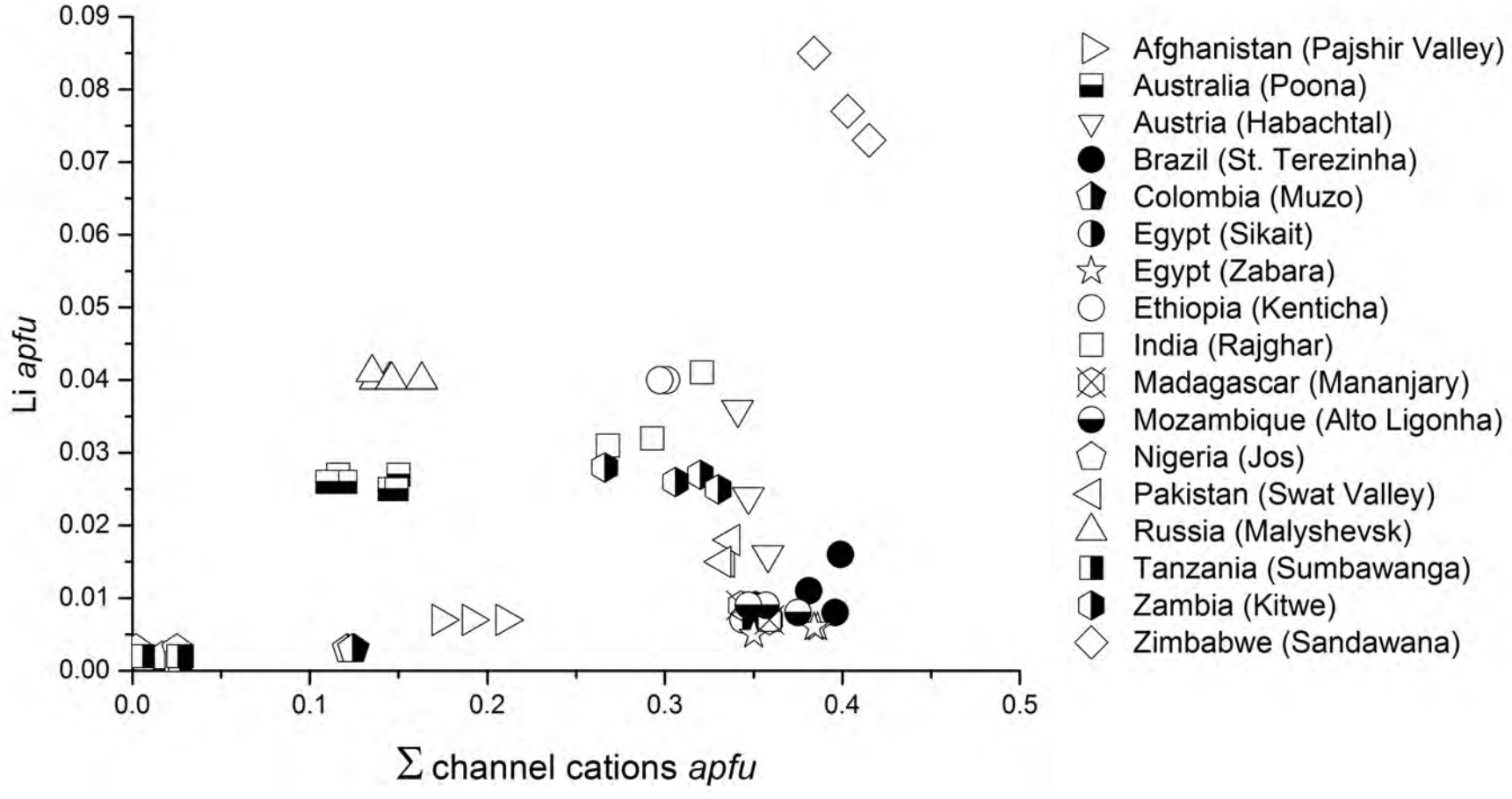
0.09
0.08
0.07
0.06
0.05
0.04
0.03
0.02
0.01
0.00
Li apfu
0.0
0.1
0.2
0.3
0.4
0.5
Σ channel cations apfu
Afghanistan (Pajshir Valley)
Australia (Poona)
Austria (Habachtal)
Brazil (St. Terezinha)
Colombia (Muzo)
Egypt (Sikait)
Egypt (Zabara)
Ethiopia (Kenticha)
India (Rajghar)
Madagascar (Mananjary)
Mozambique (Alto Ligonha)
Nigeria (Jos)
Pakistan (Swat Valley)
Russia (Malyshevsk)
Tanzania (Sumbawanga)
Zambia (Kitwe)
Zimbabwe (Sandawana)

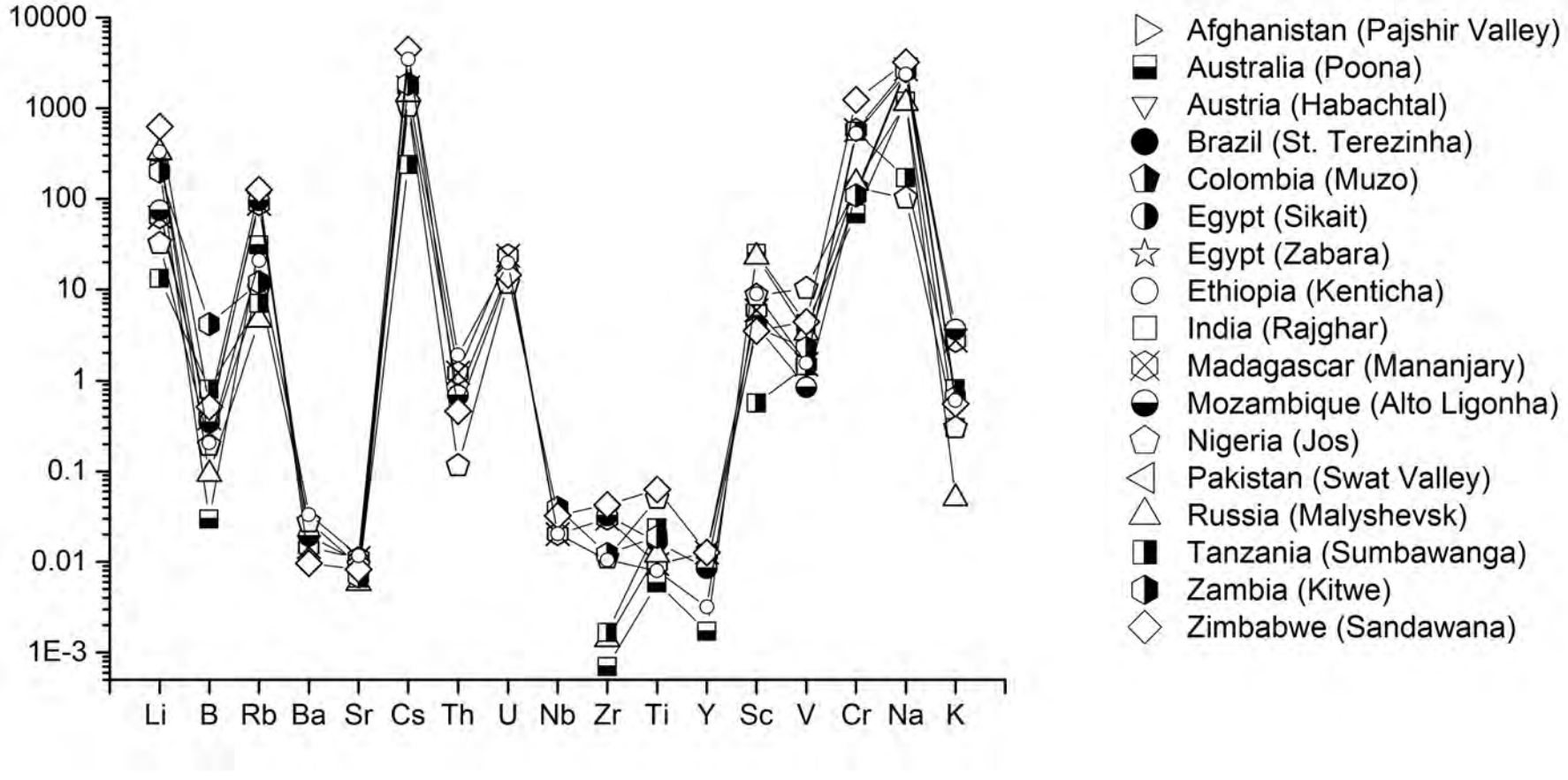
10000
1000
100
10
1
0.1
0.01
1E-3
Li
B
Rb
Ba
Sr
Cs
Th
U
Nb
Zr
Ti
Y
Sc
V
Cr
Na
K
Afghanistan (Pajshir Valley)
Australia (Poona)
Austria (Habachtal)
Brazil (St. Terezinha)
Colombia (Muzo)
Egypt (Sikait)
Egypt (Zabara)
Ethiopia (Kenticha)
India (Rajghar)
Madagascar (Mananjary)
Mozambique (Alto Ligonha)
Nigeria (Jos)
Pakistan (Swat Valley)
Russia (Malyshevsk)
Tanzania (Sumbawanga)
Zambia (Kitwe)
Zimbabwe (Sandawana)

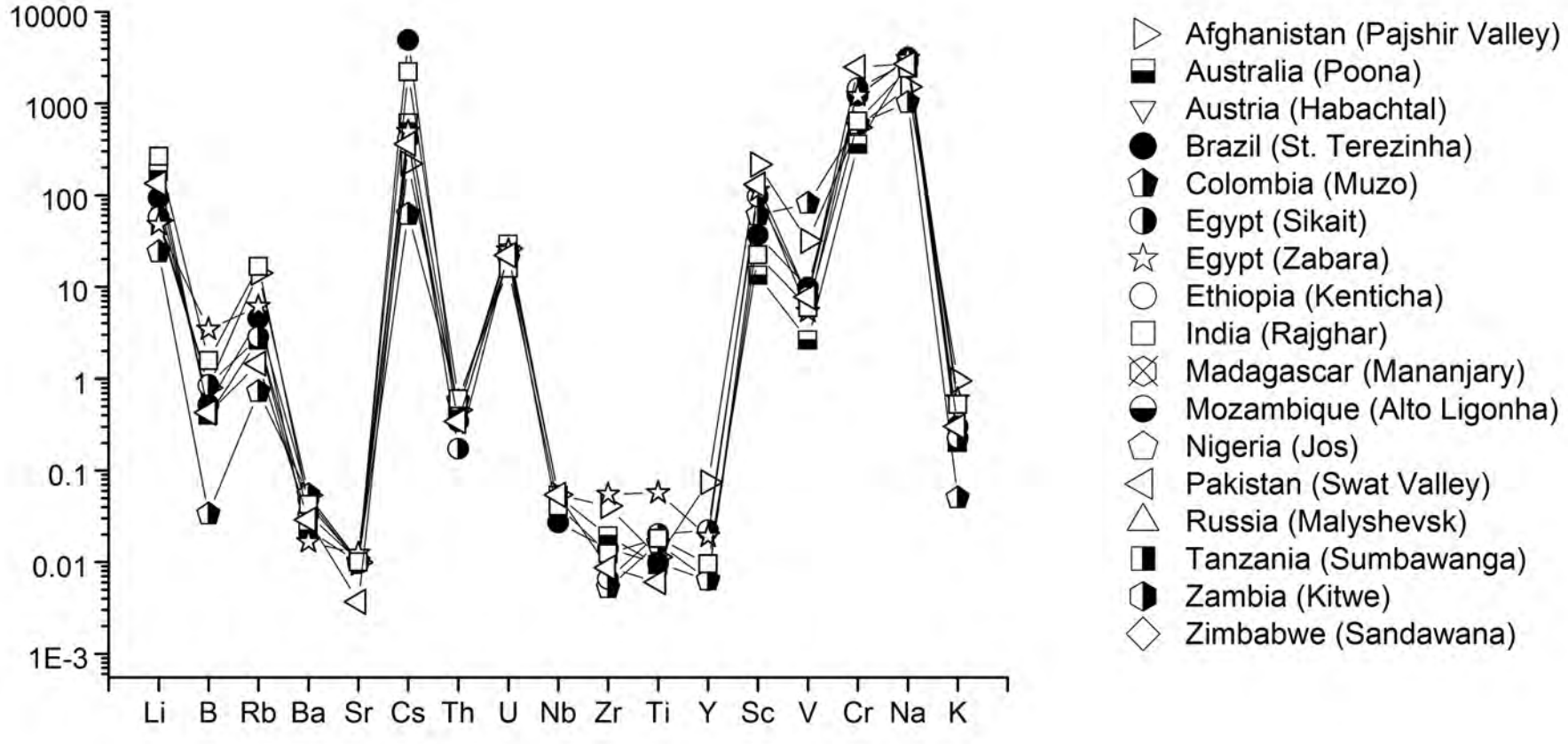
10000
1000
100
10
1
0.1
0.01
1E-3
Li
B
Rb
Ba
Sr
Cs
Th
U
Nb
Zr
Ti
Y
Sc
V
Cr
Na
K
Afghanistan (Pajshir Valley)
Australia (Poona)
Austria (Habachtal)
Brazil (St. Terezinha)
Colombia (Muzo)
Egypt (Sikait)
Egypt (Zabara)
Ethiopia (Kenticha)
India (Rajghar)
Madagascar (Mananjary)
Mozambique (Alto Ligonha)
Nigeria (Jos)
Pakistan (Swat Valley)
Russia (Malyshevsk)
Tanzania (Sumbawanga)
Zambia (Kitwe)
Zimbabwe (Sandawana)

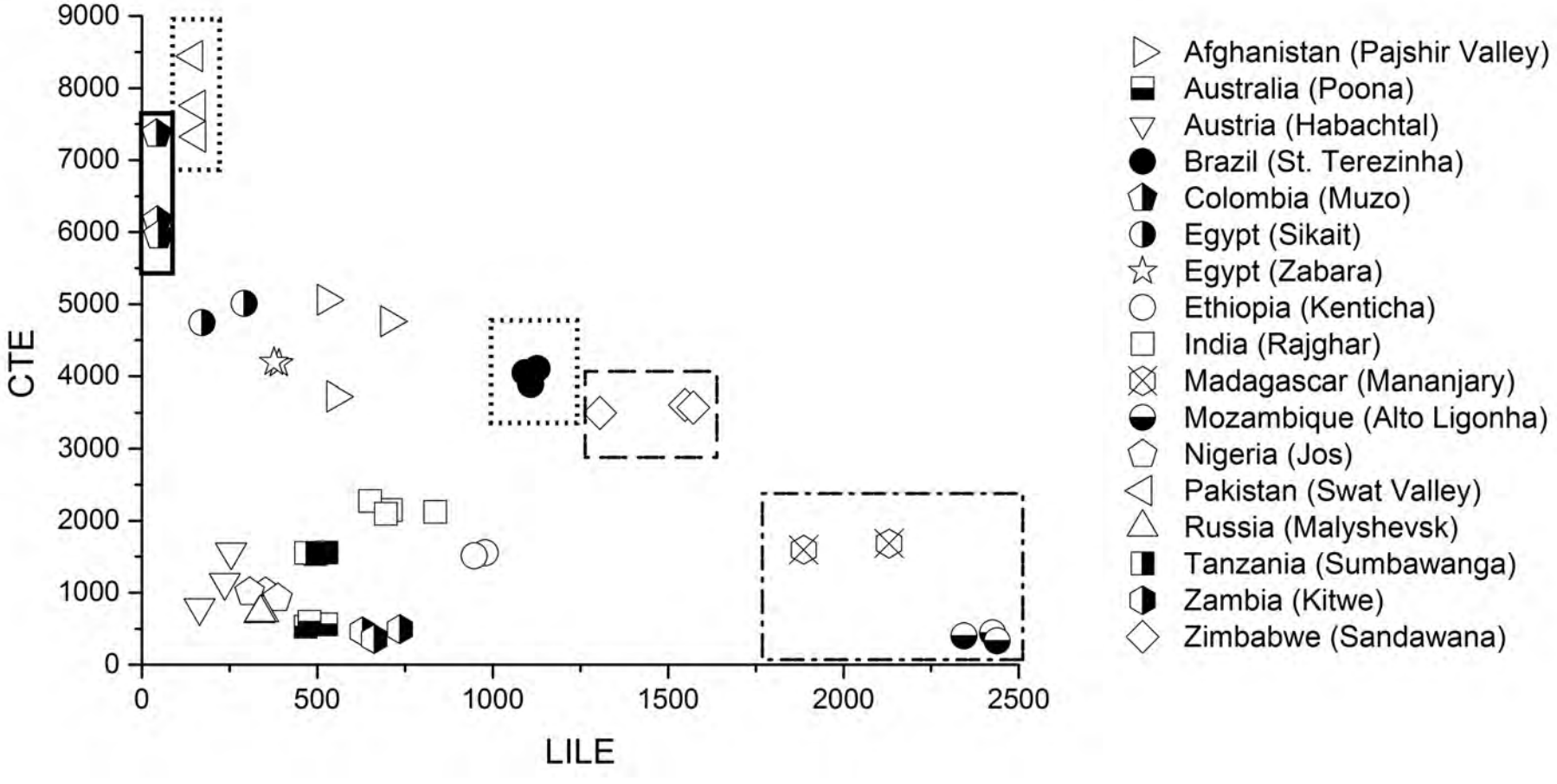
9000
8000
7000
6000
5000
4000
3000
2000
1000
0
CTE
0
500
1000
1500
2000
2500
LILE
Afghanistan (Pajshir Valley)
Australia (Poona)
Austria (Habachtal)
Brazil (St. Terezinha)
Colombia (Muzo)
Egypt (Sikait)
Egypt (Zabara)
Ethiopia (Kenticha)
India (Rajghar)
Madagascar (Mananjary)
Mozambique (Alto Ligonha)
Nigeria (Jos)
Pakistan (Swat Valley)
Russia (Malyshevsk)
Tanzania (Sumbawanga)
Zambia (Kitwe)
Zimbabwe (Sandawana)

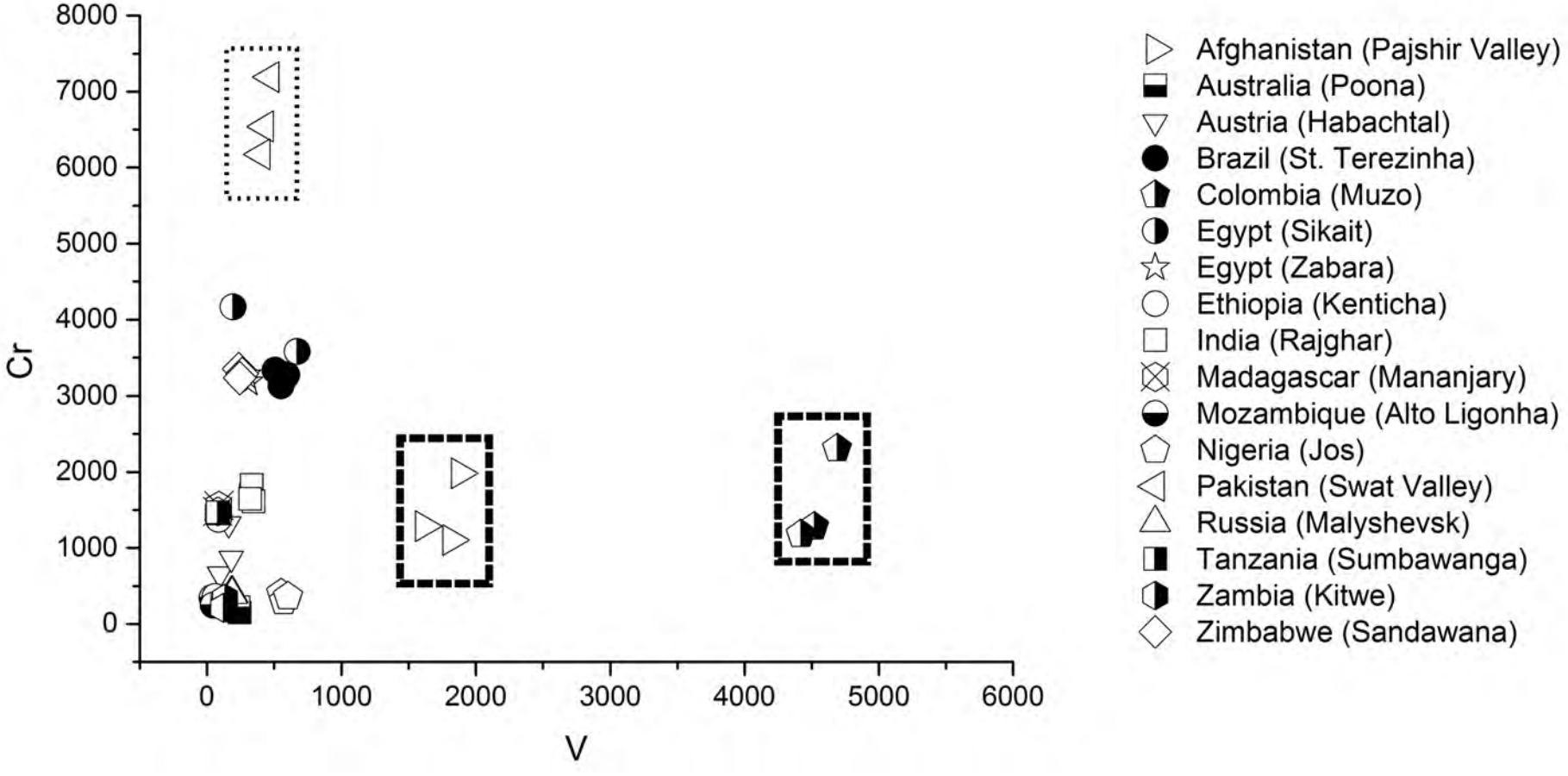
8000
7000
6000
5000
4000
3000
2000
1000
0
Cr
0
1000
2000
3000
4000
5000
6000
V
Afghanistan (Pajshir Valley)
Australia (Poona)
Austria (Habachtal)
Brazil (St. Terezinha)
Colombia (Muzo)
Egypt (Sikait)
Egypt (Zabara)
Ethiopia (Kenticha)
India (Rajghar)
Madagascar (Mananjary)
Mozambique (Alto Ligonha)
Nigeria (Jos)
Pakistan (Swat Valley)
Russia (Malyshevsk)
Tanzania (Sumbawanga)
Zambia (Kitwe)
Zimbabwe (Sandawana)

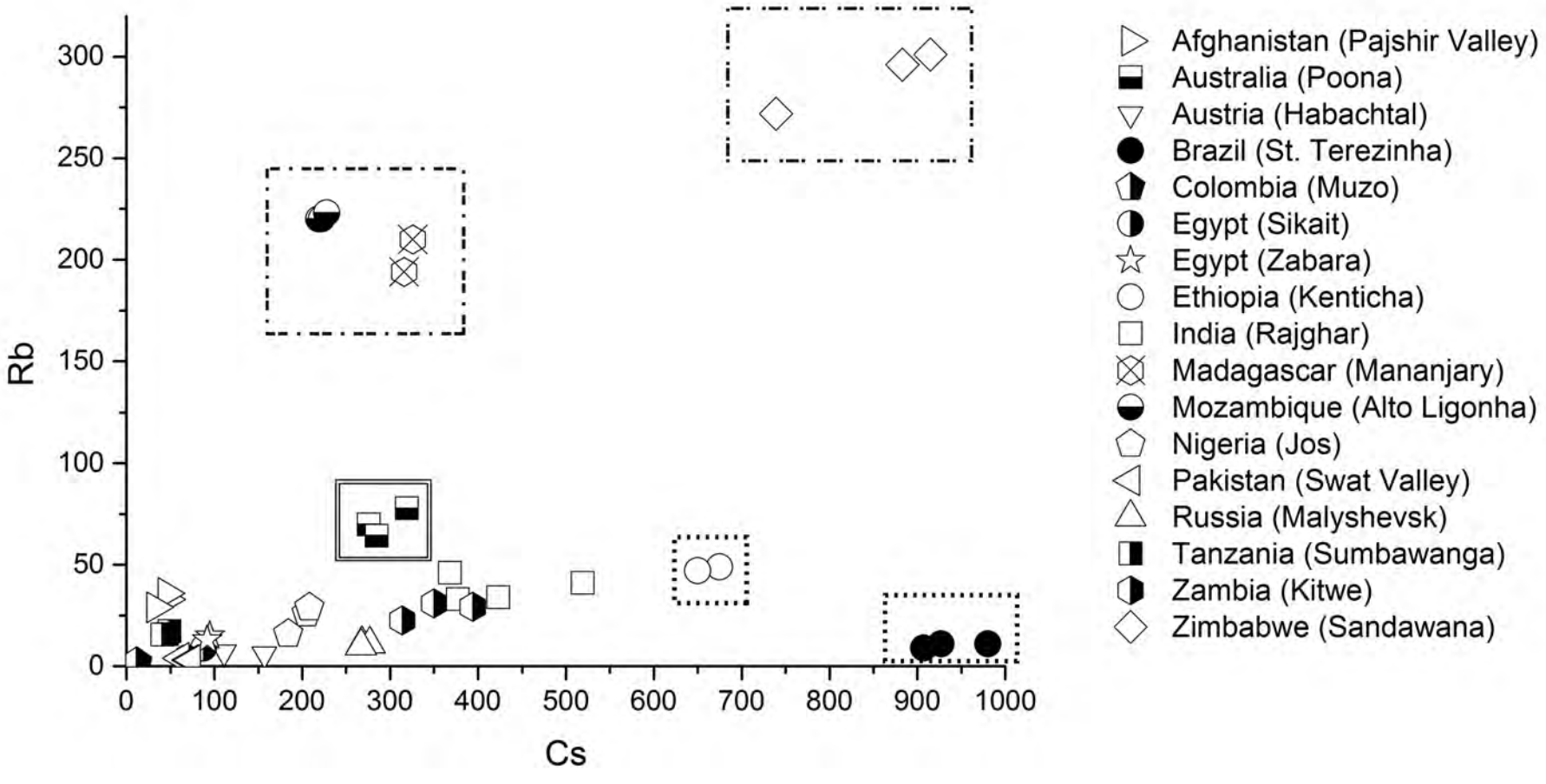
Rb
Cs
0
50
100
150
200
250
300
0
100
200
300
400
500
600
700
800
900
1000
Afghanistan (Pajshir Valley)
Australia (Poona)
Austria (Habachtal)
Brazil (St. Terezinha)
Colombia (Muzo)
Egypt (Sikait)
Egypt (Zabara)
Ethiopia (Kenticha)
India (Rajghar)
Madagascar (Mananjary)
Mozambique (Alto Ligonha)
Nigeria (Jos)
Pakistan (Swat Valley)
Russia (Malyshevsk)
Tanzania (Sumbawanga)
Zambia (Kitwe)
Zimbabwe (Sandawana)

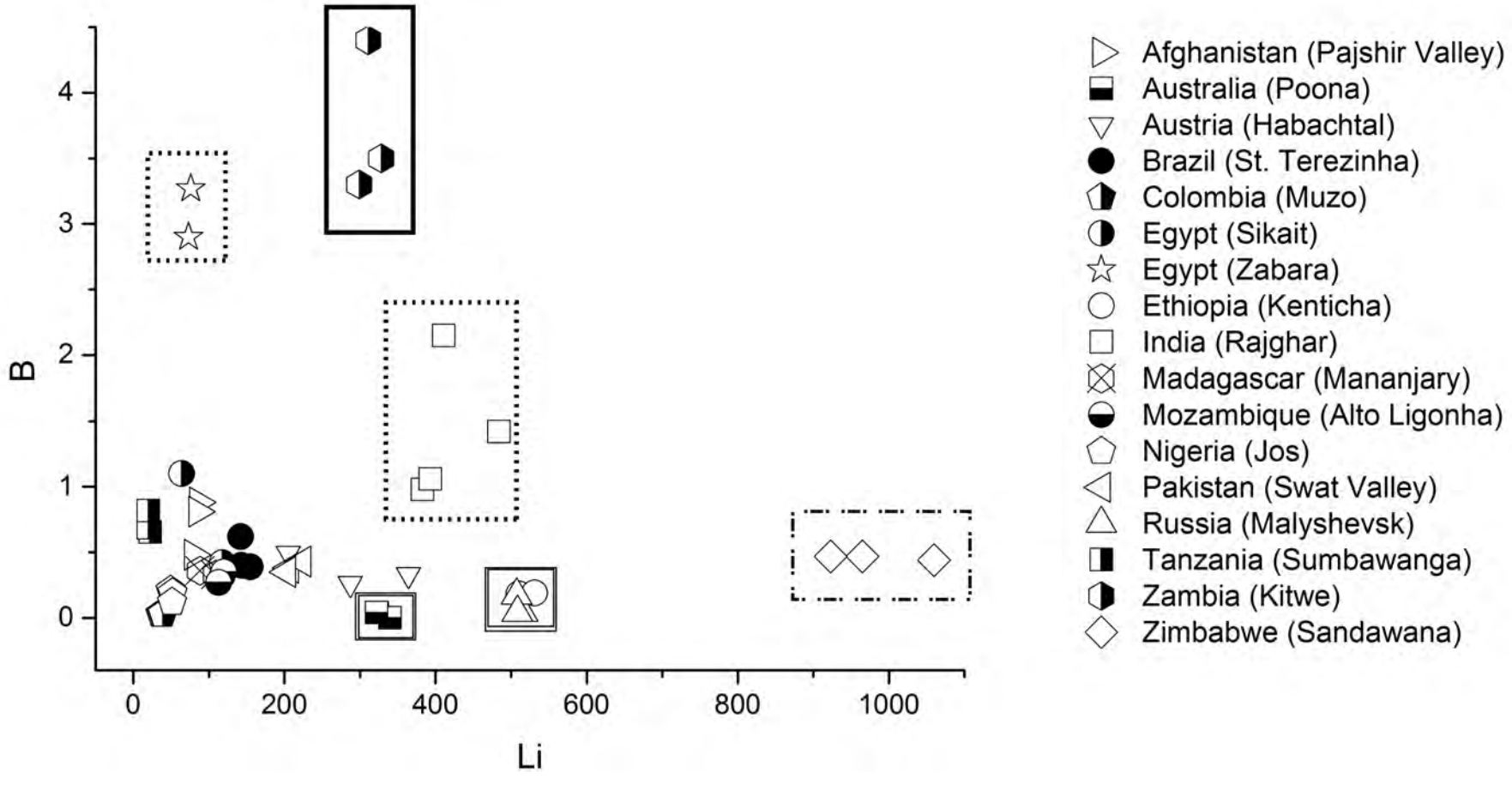
B
Li
0
1
2
3
4
0
200
400
600
800
1000
Afghanistan (Pajshir Valley)
Australia (Poona)
Austria (Habachtal)
Brazil (St. Terezinha)
Colombia (Muzo)
Egypt (Sikait)
Egypt (Zabara)
Ethiopia (Kenticha)
India (Rajghar)
Madagascar (Mananjary)
Mozambique (Alto Ligonha)
Nigeria (Jos)
Pakistan (Swat Valley)
Russia (Malyshevsk)
Tanzania (Sumbawanga)
Zambia (Kitwe)
Zimbabwe (Sandawana)

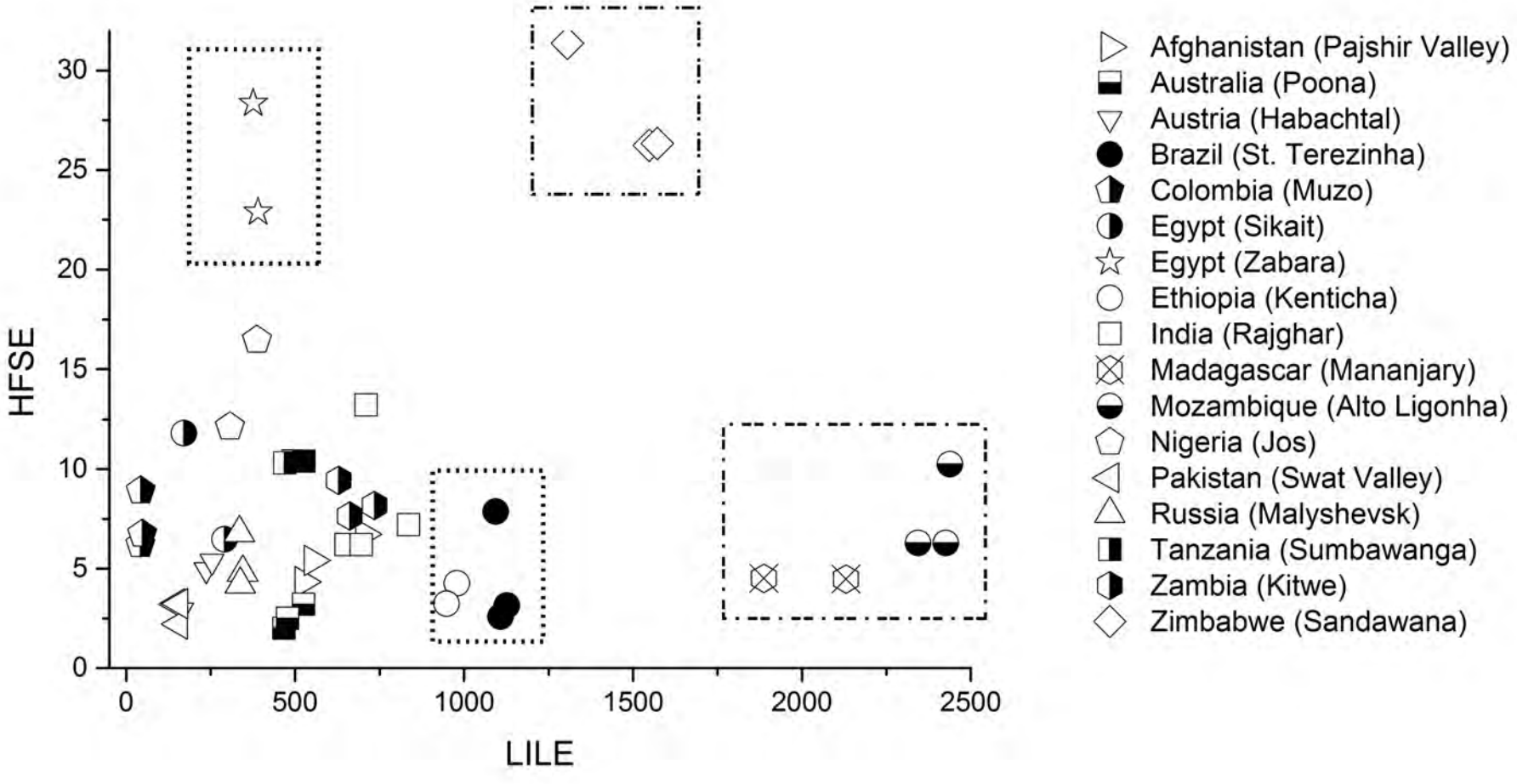
HFSE
LILE
0
5
10
15
20
25
30
0
500
1000
1500
2000
2500
Afghanistan (Pajshir Valley)
Australia (Poona)
Austria (Habachtal)
Brazil (St. Terezinha)
Colombia (Muzo)
Egypt (Sikait)
Egypt (Zabara)
Ethiopia (Kenticha)
India (Rajghar)
Madagascar (Mananjary)
Mozambique (Alto Ligonha)
Nigeria (Jos)
Pakistan (Swat Valley)
Russia (Malyshevsk)
Tanzania (Sumbawanga)
Zambia (Kitwe)
Zimbabwe (Sandawana)

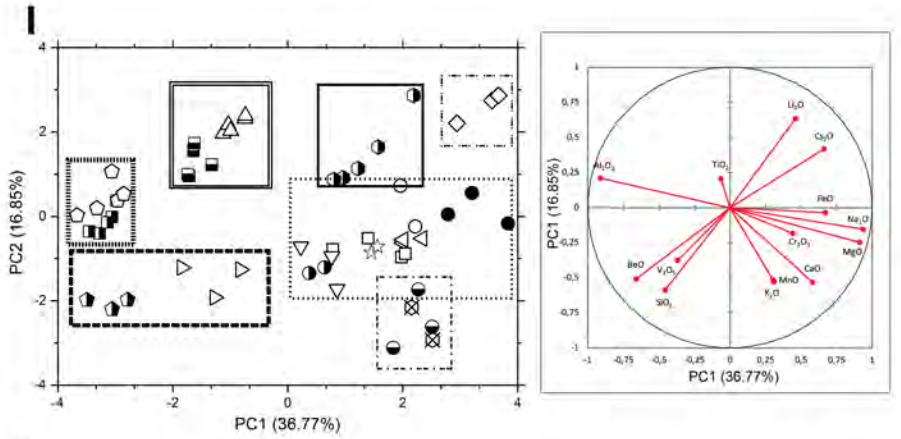

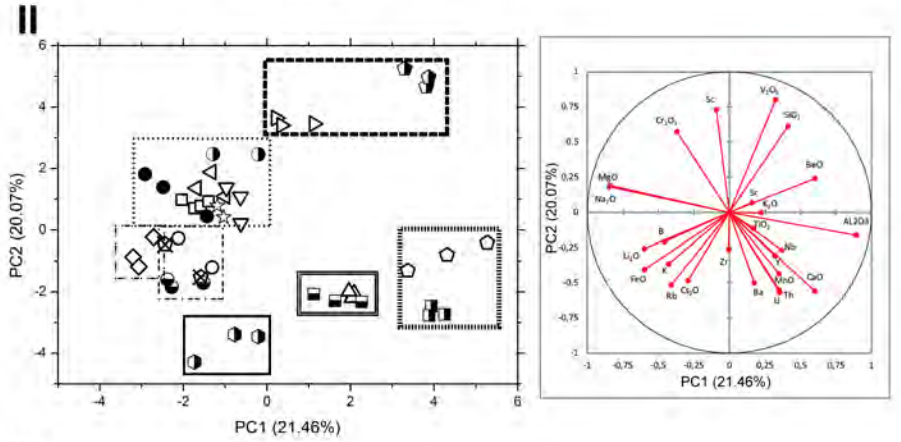

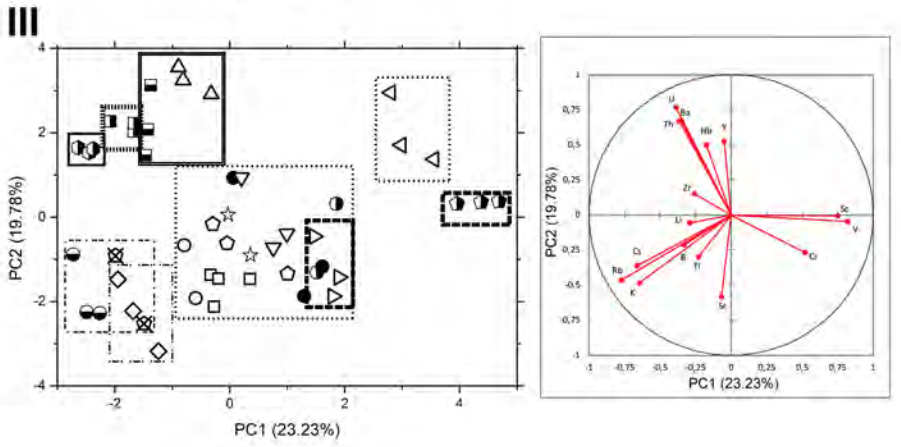

- Afghanistan (Pajshir Valley)
- Australia (Poona)
- Austria (Habachtal)
- Brazil (St. Terezinha)
- Colombia (Muzo)
- Egypt (Sikait)
- Egypt (Zabara)
- Ethiopia (Kenticha)
- India (Rajghar)
- Madagascar (Mananjary)
- Mozambique (Alto Ligonha)
- Nigeria (Jos)
- Pakistan (Swat Valley)
- Russia (Malyshevsk)
- Tanzania (Sumbawanga)
- Zambia (Kitwe)
- Zimbabwe (Sandawana)